IOWA STATE UNIVERSITY
Digital Repository

2009

Response of tin whiskers to dynamic input: Mathematical modeling and experimental property measurement

Matthew James Spitzner
Iowa State University

Follow this and additional works at: https://lib.dr.iastate.edu/etd

Part of the Mechanical Engineering Commons

Response of tin whiskers to dynamic input: Mathematical modeling and experimental property measurement

by

Matthew James Spitzner

A thesis submitted to the graduate faculty

in partial fulfillment of the requirements for the degree of

MASTER OF SCIENCE

Major: Mechanical Engineering

Program of Study Committee:
Pranav Shrotriya, Major Professor
Sriram Sundararajan
Palaniappa Molian
Frank Peters

Iowa State University

Ames, Iowa

2009

Table of Contents

List of Figures

List of Tables

Abstract

The growing risk that tin whiskers pose to the reliability of electronic assemblies has driven the need for a risk assessment tool. In this paper a mathematical model has been developed to calculate the displacement and stress response of a tin whisker to a harmonic input. The model is based on Euler-Bernoulli beam theory and utilizes the method of eigenfunction expansion to calculate the forced response solution. The model was then coded into Matlab to calculate numerical solutions for a variety of parameters. To enhance the accuracy of the model tin whisker samples were prepared and measured with a microtribometer. The whiskers were loaded traversly with a rigid probe tip and the normal and tangential forces were measured. The whiskers appeared very rigid and did not grossely fracture remaining attached to the substrate. They deformed near the root or in the surrounding tin plating where the whisker grew. The mean deformation stress calculated was 505 MPa although there were not enough measurements for statistical significance. The range of values was quite large relative to the mean. The high variability was primarily attributed to the small sample size of 3 valid measurements, the small magnitude of the forces relative to the tolerance of the microtribometer and the crystal orientation of the whisker itself.

1.   Introduction

Tin whiskers are very pure crystalline tin structures found growing from electrodeposited tin surfaces [1]. With growth potential exceeding that of lead pitch on modern electronics, and the ability to create electrical shorts they represent an ever growing risk to the functionality and long term reliability of military electronics.

Figure 1 Tin whisker growing on the inside of a mounting hole

1.1   History

Tin whiskers and the phenomenon of metal whiskers in general are not new. The first reported case of the phenomenon was in 1946. Cadmium whiskers were causing electrical shorts in World War II era military equipment. Tin and Zinc platings were used in lieu of cadmium but in 1952 these plating were also found to exhibit the whisker phenomenon. In the 50s and 60s Bell Labs experimental with alloying tin to prevent whisker growth and found that 0.5% to 1% lead by weight inhibited whisker growth in tin coatings [2]. Following failures in the late 80s and early 90s attributed to tin whiskers, the US military

started prohibiting the use of pure tin in military electronics [3]. Recently however governing bodies in Japan and Europe have pushed initiatives to reduce the use of hazardous materials such as lead, the primary alloy element for tin plating [1]. As of 2006 the European Union has fully enacted the legislation Reduction of certain Hazardous Materials (RoHS) and Waste Electronic and Electrical Equipment (WEEE) requiring the most lead be removed from electronic equipment [4]. This has lead to electronic component manufacturers replacing more traditional tin-lead alloy plating with pure tin plating. Pure tin plating carries with it excellent corrosion resistance, and solderability attributes as well as being relatively simple to adapt a tin-lead system to. The vast majority of component vendors seeking to meet RoHS and WEEE standards have switched to pure tin plating because of these desirable attributes.

1.2   Attributes

As previously stated tin whiskers are long crystalline filaments that grow from tin plated surfaces. They have been reported in many shapes such as straight, kinked, spiral, nodules and hillocks [5]. A very unique shaped whisker is shown in figure 2. They can grow as long as 10 mm but are found far more commonly at lengths of 1 mm or less [1],[2]. Their diameter can range from .006 μm to 10 μm, but are more typically observed at 1-4 μm. Striations can be seen running the length of the whisker so the true cross section is best described as a rosette [6]. Growth rates of whiskers are reported to be .03-9 mm per year, with growth densities from single whiskers to 104 per square centimeters. Mechanical properties have been reported to be high in the axial direction due to the high purity crystalline structure, but low in the shear direction. Whiskers also have the ability to carry currents of up to 75 mA continuously depending on diameter, and much high then this momentarily before fusing due to the heat generated[1].
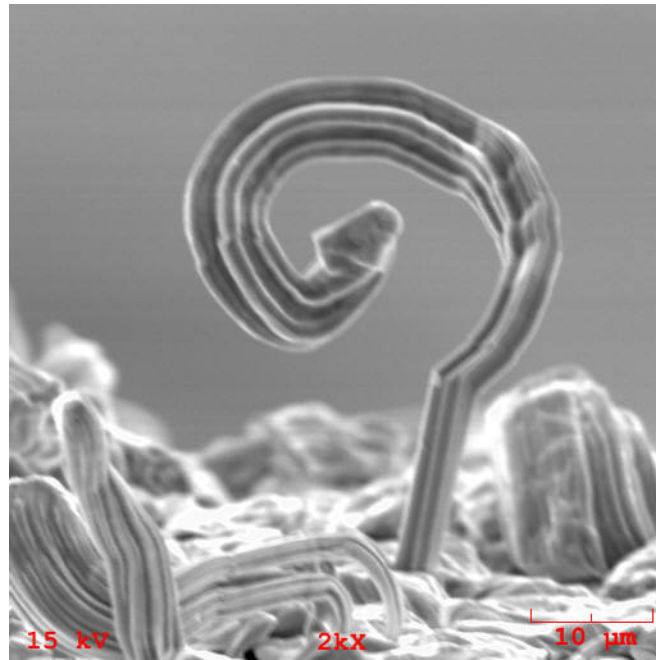
Figure 2 A "?" shaped tin whisker (spiral type)

1.3　　Growth Mechanism

Although no specific mechanism is known to cause whisker growth there are many factors that are generally agreed upon that contribute to whisker growth, as well as some agreed to not influence the growth. Growth contributors are: residual stress in the tin plating, compressive stressed such as those imparted by a screw or substrate deformation, stresses induced by thermal cycling, temperature raging from 50 to 140 Celsius, and organic additives use in bright tin plating. Whiskers have been shown to grow regardless of factors such as applied current, or electric field, moisture or atmospheric pressure [3]. One thing that is know about the growth of whiskers is the growth occurs from the base of the whisker like an extrusion rather that at the tip like more traditional crystal formation. Additionally the tin local to the whisker is not depleted by its growth indicating that the growth is fed by a diffusion mechanism through or across the lattice of the plating. Recent tests using tin isotopes as tracers and Secondary Ion Mass Spectroscopy (SIMS) has shown that there is a long range diffusion of tin across the surface lattice of the plating to the site of the whisker, and relatively little diffusion through the body lattice [7].

1.4   Risks

There are 4 primary risks posed by growth of tin whiskers in electronic assemblies. The first is continuous short circuiting in low current applications (< 50 mA). The second is transient shorting of higher current applications (> 50 mA). Whiskers have been shown to cause momentary glitches in higher current applications before fusing open. The third is contamination or interference with sensitive components in the assembly. If a whisker breaks loose of its substrate it may travel throughout the enclosure and impede the functionality of sensitive optics or micro and nano-electromechanical systems. The fourth if by far the more dangerous and spectacular risk however it requires a space based application. In a vacuum a whisker that shorts a high current circuit may vaporize and form a metal vapor, or plasma. This plasma is capable of caring hundreds of amperes of current continuously and can lead to total system failure and gross destruction of entire electronic enclosures. Metal vapor arcing of a tin whisker has been attributed as the failure of 3 commercial satellites [1], [3].
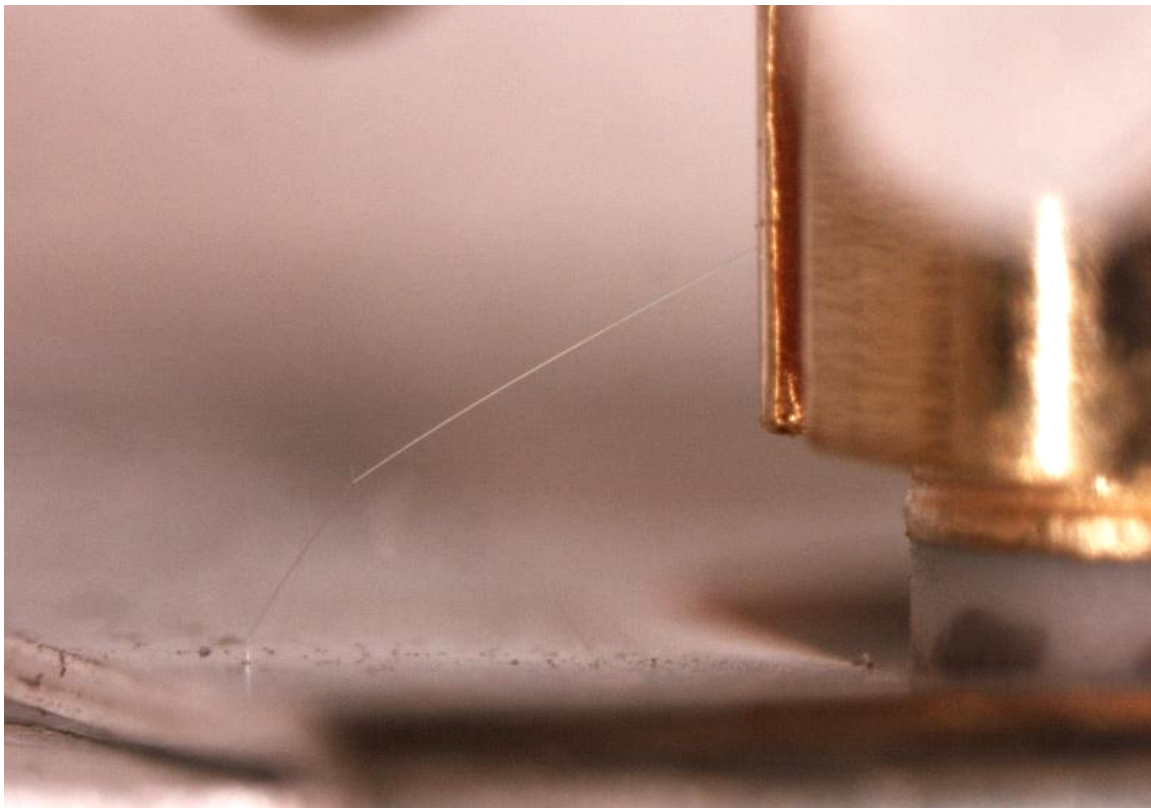
Figure 3 Electrical short casued by a 2mm long tin whisker

1.5   Risk Analysis

Due to the hazards that tin whiskers present to electronic assemblies it becomes necessary to assess the risk to a system if tin whiskers are discovered to be growing. This has occurred on legacy products when the risk of tin whiskers was not mitigated. It has also occurred when tin plating chemistry went out of specification, resulting in plating with insufficient alloying elements to inhibit whisker growth. Various considerations can be made with regards to geometry of whiskers and components, as well as severity of failures if a whisker were to short a circuit. An important factor that is hard to quantify is the risk that a whisker will break free of its substrate given a particular geometry and environment of dynamic inputs such as mechanical shock and vibration. To assess this risk a model of the whiskers' dynamic response and stress levels must be developed. Additionally whisker properties such as modulus of elasticity and ultimate strength must be know with enough accuracy to render the model useful.

2.   Tin Whisker Modeling

2.1   Introduction

To determine the modeling method most suited to that of a tin whisker the basic requirements of the model were listed.

1.   Model should yield displacements of the whisker for use in stress calculations

2.   Model should be able to handle various forced inputs, particularly harmonic inputs

3.   Model should be implemented in a software package to make then analysis of varying geometries, or inputs simple to recalculate.

Review of the literature revealed substantial work in the area of tin whiskers, but all of it related to growth theories and mitigation techniques. Work related to modeling the physical response of whiskers to dynamic inputs was not found.

Inspection of the parameters of a typical tin whisker reveals very long, thin, straight structures, with basically uniform cross-sections attached free standing to a substrate. The intuitive choice was to model the whisker as a cantilevered beam of uniform cross section. An abundance of literature exists on various theories and methods to model traversely vibrating beams such as: Euler-Bernoulli[8], Rayleigh[9], Shear[9], Timoshenko [10], [11], as well as more specific applications such as simplifications of Timoshenko theory to reduce computational effort [12] among others. Han, Benaroya and Wei [9] present a complete development of four engineering theories including the most widely used, the Euler-Bernoulli and Timoshenko Beam theories. The Euler-Bernoulli theory also know as the classic beam theory, is simple and generally provides reasonable engineering estimated of displacement especially in longer, slender beams. It is based on the single largest factor in beam displacement, bending moment, while ignoring other effects. The Timoshenko theory improves upon the Euler-Bernoulli theory my adding the effect of shear and rotation. This is especially important for non slender beams where the effects of shear and rotation are more dominant in the governing equation. Han et al has compiled and compared the frequency curves for all for theories and recommend that when slenderness ratio is larger then 100 the Euler-Bernoulli model can be used with similar results to the other models, where as beams

with lower slenderness ratios should be handled with the Shear or Timoshenko theory to maintain high accuracy. Since tin whiskers are generally 1-4 μm in diameter and up to 1000 μm or longer, the slenderness ratio of whiskers that pose the greatest risk to electronic components will also have slenderness ratios greater than 100. For this reason the Euler-Bernoulli beam theory was chosen. The full derivation of the governing equation using Euler-Bernoulli is available in many text books [13, 14] and will not be shown here. The governing equation is a linear fourth order non-homogeneous partial differential equation. The basic technique used to solve this will be eigenfunction expansion, also known as mode superposition. The homogeneous form of the governing equation will be solved yielding eigenvalues and eigenfunctions of the problem. Then time based functions, called principle coordinates will be determined and used in conjunction with the eigenfunctions to formulate the total solution.

2.2   Modeling

2.2.1   *Governing Equation*

Starting with the Euler-Bernoulli governing equation for elastic bending of a beam gives

$$\rho A \frac{\partial^2 u}{\partial t^2} - \mu \frac{\partial^2 u}{\partial x^2} + \frac{\partial^2}{\partial x^2}\left(EI \frac{\partial^2 u}{\partial x^2} \right) = f(x,t) .$$
(1)

Inspection of whisker geometry shows the cross-section to be independent of length. Assuming the modulus of elasticity is also independent of length yields

$$\rho A \frac{\partial^2 u}{\partial t^2} - \mu \frac{\partial^2 u}{\partial x^2} + EI \frac{\partial^4 u}{\partial x^4} = f(x,t) .$$
(2)

Taking the homogeneous form of equation 2 and neglecting the tension in the beam (μ=0) we can rewrite

$$\frac{\partial^2 u}{\partial t^2} + c^2 \frac{\partial^4 u}{\partial x^4} = 0 ,$$
(3)

where the constants have been combined into a single value defined as

$$c = \sqrt{\frac{EI}{\rho A}} \tag{4}$$

2.2.2 Separation of Variables

Equation 3 is a separable differential question and can be solved by assuming a solution of the form

$$u(x,t) = T(t)U(x) \tag{5}$$

Substituting equation 5 into equation 3 and rearranging yields

$$\frac{c^2}{U(x)} \frac{\partial^4 U(x)}{\partial x^4} = -\frac{1}{T(t)} \frac{\partial^2 T(t)}{\partial t^2} \tag{6}$$

Since both sides of equation 6 are equal, they must also be equal to a constant. Setting both sides of equation 6 equal to a constant; further simplifications are made to complete the separation of variables

$$\frac{\partial^4 U(x)}{\partial x^4} - \beta^4 U(x) = 0, \qquad \frac{\partial^2 T(t)}{\partial t^2} + \omega^2 T(t) = 0 \tag{7, 8}$$

where the constants have again been combined into a single value defined as

$$\beta^4 = \frac{\omega^2}{c^2} \tag{9}$$

2.2.3 Homogeneous Solution

The general solution to equations 7 and 8 are given by:

$$U(x) = a_0 \sin \beta x + a_1 \cos \beta x + a_2 \sinh \beta x + a_3 \cosh \beta x \tag{10}$$

$$T(t) = a_4 \sin \omega t + a_5 \cos \omega t \tag{11}$$

where a_i are constant coefficients. The boundary and initial conditions are used to solve for the unknown coefficients. In this case we are only interested in the spatial solution, as it will yield the eigenvalues and eigenfunctions used in the non-homogeneous problem.

Boundary conditions for a cantilever beam are clamped at the base with zero displacement or slope and free at the opposite end with no moment or shear. These boundary conditions are written

$$U(0) = \frac{\partial U(0)}{dx} = \frac{\partial^2 U(l)}{dx^2} = \frac{\partial^3 U(l)}{dx^3} = 0 \qquad (12)$$

Substituting equation 12 into equation 10 will yield four simultaneous equations that can be assembled into matrix form

$$\begin{bmatrix} 0 & 1 & 0 & 1 \\ 1 & 0 & 1 & 0 \\ -\sin(\beta l) & -\cos(\beta l) & \sinh(\beta l) & \cosh(\beta l) \\ -\cos(\beta l) & \sin(\beta l) & \cosh(\beta l) & \sinh(\beta l) \end{bmatrix} \begin{bmatrix} a_0 \\ a_1 \\ a_2 \\ a_3 \end{bmatrix} = \begin{bmatrix} 0 \\ 0 \\ 0 \\ 0 \end{bmatrix} \qquad (13)$$

Since we are only interested in the non-trivial solutions to equation 13 we set the determinant of the 4 x 4 matrix equal to zero and simplify yielding the frequency equation

$$\cos(\beta l)\cosh(\beta l) + 1 = 0 \qquad (14)$$

The frequency equation has an infinite number of solutions called eigenvalues. The first three solutions representing the first three modes of natural frequency are shown in table 1. These values have been verified in reference 9 and 14.

Table 1 First 5 eigenvalues

n	_1_	_2_	_3_	_4_	_5_
$\beta_n l$	_1.8751_	_4.6941_	_7.8548_	_10.9955_	_14.1372_

For each eigenvalue there is an associated eigenfunction, a unique set of coefficents a_i, and a natural frequency that can be determined from equation 9. To determine the eigenfunctions the coefficients of equation 13 can be reduced from four to one and gives a simple form

$$U_n(x) = a_n \left[\left(\sin \beta_n x - \sinh \beta_n \right) - \alpha_n \left(\cos \beta_n - \cosh \beta_n \right) \right], \qquad (15)$$

Where coefficient α_n is defined as

$$\alpha_n = \left(\frac{\sin \beta_n l + \sinh \beta_n l}{\cos \beta_n l + \cosh \beta_n l} \right), \qquad (16)$$

and the index n represents correlation with the "nth" eigenvalue.

An important property of eigenfunctions that will prove useful is orthogonally. The full derivation of orthogonally of eigenfunctions is presented in reference 9 and the resulting equation is

$$\int_0^l U_m(x)^{\mathrm{T}} U_n(x)\, dx = \delta_{mn},$$
(17)

where δmn is the kronecker delta.

2.2.4 Non-homogeneous Solution

Reverting to the non-homogeneous governing equation 2 and again neglecting tension in the beam yields

$$\rho A \frac{\partial^2 u}{\partial t^2} + EI \frac{\partial^4 u}{\partial x^4} = f(x,t).$$
(18)

For the method of eigenfunction expansion assume a solution of a series summation of temporal and spatial functions. Specifically the spatial forms are the eigenfunctions found in the homogeneous solution and are combined with the temporal functions to yield the total solution

$$u(x,t) = \sum_{n-1}^{\infty} \eta_n(t) \cdot U_n(x).$$
(19)

Although the assumed solution looks similar to equation 5 the non-homogeneous governing equation is no longer separable so a new technique must be employed to find the temporal solutions. Substituting equation 19 into equation 18 yields

$$\sum_{n-1}^{\infty} U_n(x) \cdot \rho A \frac{\partial^2 \eta_n(t)}{dt^2} + \sum_{n-1}^{\infty} \eta_n(t) \cdot EI \frac{\partial^4 U_n(x)}{dx^4} = f(x,t).$$
(20)

At this point equation 7 developed in the homogeneous solution can be brought back and rewrote to yield

$$EI \cdot \frac{\partial^4 U(x)}{\partial x^4} = \omega_n^{\,2} \cdot \rho A \cdot U(x).$$
(21)

Substituting equation 21 into equation 20 yields the following simplification now with only first order spatial functions

$$\sum_{n-1}^{\infty} U_n(x) \cdot \frac{\partial^2 \eta_n(t)}{dt^2} + \sum_{n-1}^{\infty} \eta_n(t) \cdot \omega_n^2 \cdot U(x) = \frac{1}{\rho A} f(x,t) \tag{22}$$

Since equation 22 now contains only first order eigenfunctions, the orthogonally condition can be used to decouple the principle coordinates. Multiplying the equation 22 by $U_m(x)$ and integrating across the domain to obtain

$$\int_0^l U_m(x) \left(\sum_{n-1}^{\infty} U_n(x) \cdot \frac{\partial^2 \eta_n(t)}{dt^2} + \sum_{n-1}^{\infty} \eta_n(t) \cdot \omega_n^2 \cdot U(x) \right) = \int_0^l U_m(x) \frac{1}{\rho A} f(x,t) \tag{23}$$

which decouples the principle coordinates

$$\frac{\partial^2 \eta_n(t)}{dt^2} + \omega_n^2 \eta_n(t) = \frac{1}{\rho A} Q_n \tag{24}$$

where Qn is the generalized force which is associated with the generalized coordinate and is defined as

$$Q_n = \int_0^1 U_n(x) f(x,t) \cdot dx \tag{25}$$

We have now uncoupled the principle coordinates from the eigenfunctions. The result is a linear second order non-homogeneous differential equation that can be solved by finding a particular solution and the general solution to the homogeneous form of the equation. Since the forcing function is harmonic the solution is also assumed to be harmonic. A particular solution of the following form is assumed

$$\eta_n(t) = X \sin(\Omega t) \tag{26}$$

Substituting equation 26 into equation 24, X can be solved for

$$X = \frac{1}{\rho A \sin(\Omega t)(\omega_n^2 - \Omega^2)} Q_n \tag{27}$$

Substituting equation 27 into equation 26 and combining with the general solution to the homogeneous form of equation 24 yields the total equation for the principal coordinates

$$\eta_n = A_n \cdot \cos \omega_n t + B_n \cdot \sin \omega_n t + \frac{1}{\rho A(\omega_n^2 - \Omega^2)} Q_n \tag{28}$$

The first two terms of equation 28 represent the free vibrations resulting from initial conditions, where as the third terms represents the steady state vibrations resulting from the

forcing function. To determine the coefficients An and Bn the initial conditions must be transformed in terms of η_n. Starting with equation 19 and again multiply by $U_m(x)$ and integrating over the domain yields the relation

$$\eta_n(t) = \int_0^l U_m(x) \cdot u(x,t) \cdot dx .$$

(29)

Applying the initial conditions to equation 28 yields the following expressions

$$\eta_n(0) = \int_0^l U_m(x) \cdot u(x,0) \cdot dx, \qquad \frac{d\eta_n(0)}{dt} = \int_0^l U_m(x) \cdot \frac{du}{dt}(x,0) \cdot dx$$

(30, 31)

which can be used to solve for An and Bn.

To determine the values for An evaluate equation 28 at zero time and set the result equal to equation 30. Rearranging yields the equation for An. To determine the values of Bn follow the same procedure but take the first derivative of equation 28 and set the result equal to equation 31. Rearranging yields the equation for Bn

$$A_n = \int_0^l U_m(x) \cdot u(x,0) \cdot dx - \frac{1}{\rho A(\omega_n^2 - \omega^2)} \left[\int_0^1 U_n(x) f(x,t) \cdot dx \right]\Big|^{t=0},$$

(32)

$$B_n = \frac{1}{\omega_n} \left[\int_0^l U_m(x) \cdot \frac{du}{dt}(x,0) \cdot dx - \left[\frac{d}{dt}\left(\frac{1}{\rho A(\omega_n^2 - \omega^2)} \int_0^1 U_n(x) f(x,t) \cdot dx \right) \right]\Big|^{t=0} \right].$$

(33)

Combining the principle coordinates (equation 28) with the eigenfunctions (equation 15) into the assumed solution (equation 19), will yield the total solution to the non-homogeneous equation.

2.2.5 *Dynamic Moment and Stress*

To determine the stress on the root of the whisker the effective dynamic moment must be calculated. This is accomplished using equation 19 and the relation between moment and deflection defined by Euler-Bernoulli beam theory given by

$$M(x,t) = EI \frac{\partial^2 u}{\partial x^2} .$$

(34)

Using equation 34 and basic whisker properties the bending stress can be calculated by

$$\sigma_{bending} = \frac{M\left(x,t\right)\cdot c}{I}$$

(35)

2.3   Numerical Implementation and Optimization

To make the calculations described in the previous section manageable as well as flexible enough vary parameters such as whisker geometry, forcing function, and model parameters, the equations were coded into Matlab, a commercially available technical computing software package. The complete code is presented in appendix A. Specific details of the implementation and model optimization are discussed below.

2.3.1   Force Implementation

To numerically implement the generalized force of equation 25 the forcing function must be cast dimensionally in terms described by the governing equation. The form of the forcing is assumed to be harmonic application of Newtons at a defined frequency. One typical forcing function environment of interest to electronics design is sinusoidal vibration. Sinusoidal vibration is typically defined as an acceleration loading specified as Gravities with a dwell frequency. This condition is not given in terms of force directly. Additionally the loading is not applied directly to the whisker but rather the substrate. Since the loading is applied to the substrate one option is to treat the loading as a boundary condition, and solve as a free vibration problem. This yields a homogeneous governing equation but non-homogeneous boundary conditions. To solve this type of problem substitutions are made that result in homogeneous boundary conditions, with the governing equation reverting back to a non-homogeneous form [15]. This method, although valid, was deemed unnecessarily complex and a simpler method was used. If the forcing is applied in one direction to the substrate with a whisker at rest it can be seen that an equal and opposite reactionary inertial load will be applied to the whisker. Using this methodology the accelerations can be treated as direct inertial loads distributed along the length of the whisker.

2.3.2 Time Resolution

To plot the numerical solution to whisker displacement and stress a time variable was set to start at zero time and increase by some incremental time step. Because the frequency of forcing is typically specified from 100 to 2000 Hz [16] selection of an appropriate time step is important to capture the displacement waveform. This is similar to electrical signal processing where Nyquist sampling rate is used to capture full waveforms. Nyquist found that the ideal rate of sampling was 2 times the frequency of the wave form you are tying to measure. Practically speaking however a value slightly above will yield the best results [17, 18]. For the case of a vibrating beam, the response frequency will never be greater than the forcing function. For this reason the time step was set at 2.1 times the forcing frequency.

2.3.3 Eigenvalue Optimization

The number of eigenvalues used in the solution will affect both the accuracy of the solution and the computation time. To find the optimum balance the code was set to loop from one eigenvalue to fifty, each time finding the maximum and minimum whisker displacement at the tip. This plot can be seen in figure 4.
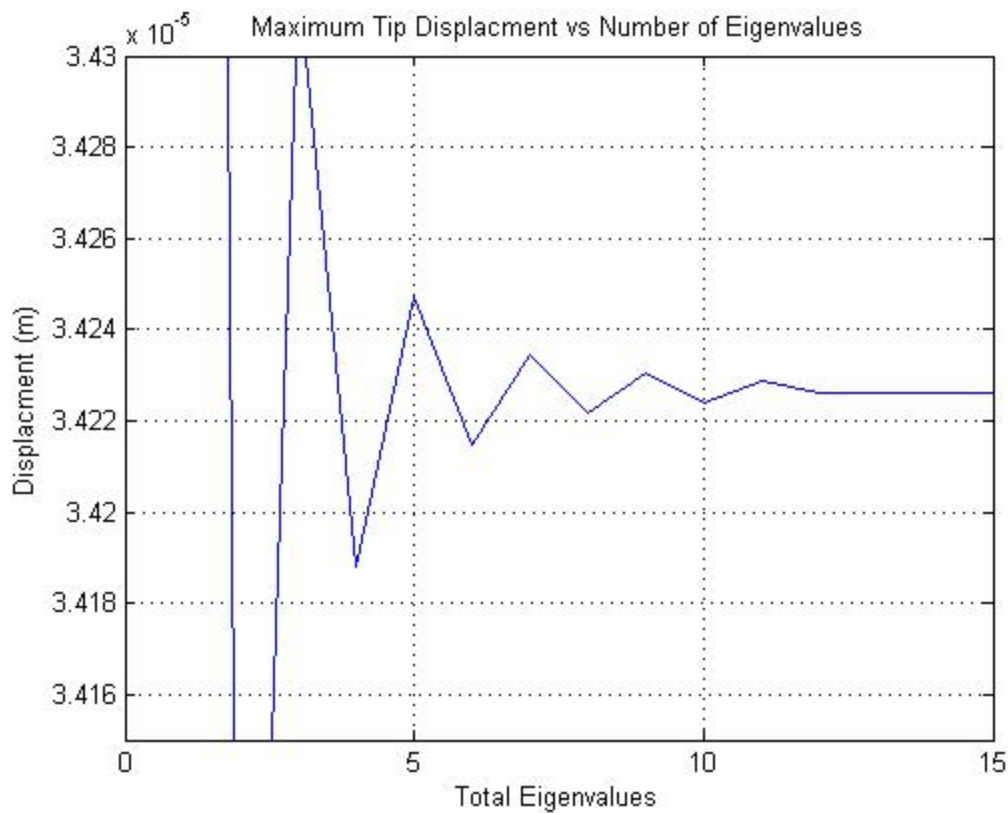
Figure 4 Convergence of displacement solution vs. eigenvalues

Since the contribution of eigenvalues beyond about 12 or 13 is insignificant the model was set to run 15 eigenvalues to optimize computation time.

2.4   Results

Results for a selected set of inputs along with parameter variation are presented.

2.4.1   *Sinusoidal Vibration Input*

The displacement and stress responses to sinusoidal inputs are presented in figures 5 and 6. The inputs used were a 5Gs dwell at 2000 Hz, and a 5G dwell at 10% below the first whisker resonance, 9777 Hz. The whisker geometry used for these results was 1 mm length and a 2 μm diameter. The density and modulus used was for that of beta phase tin.

The first run of a 5G dwell at 2000 Hz yielded maximum displacements of 15.5 μm and maximum stresses of 24.4 MPa. The response frequency of the whisker was 311.1 Hz.
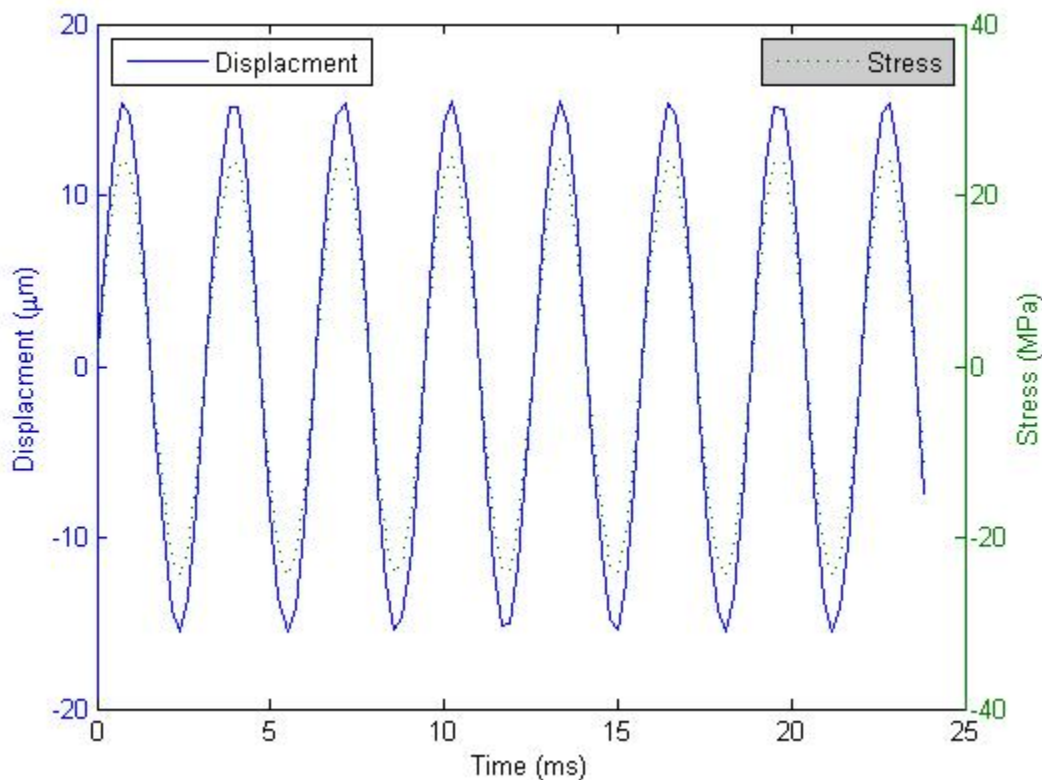

Figure 5 Displacement and stress response to 5G sinusoidal forcing at 2000 Hz

The second run of a 5G dwell at 9777 Hz, 10% below the first resonance of the 1000 μm whisker, yielded maximum displacements of 130.5 μm and maximum stresses of 113.9 MPa. The response frequency of the whisker was 1555.5 Hz.
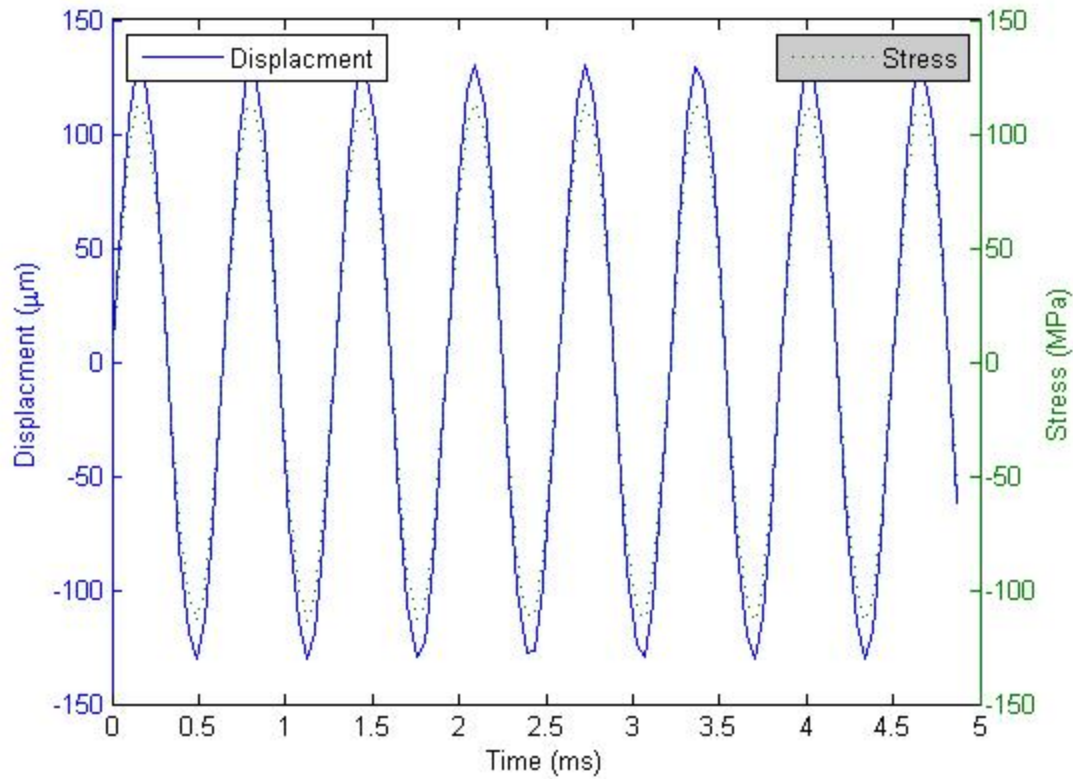
Figure 6 Displacement and stress response to 5G sinusoidal forcing at 9777 Hz

2.4.2   Parameter Variation

Next the model was reset with typical whisker values of 1000 μm length, 2 μm diameter, and 5G sinusoidal forcing at 2000Hz. Then one by one the parameters were varied to see the dependence of the displacement and the stress on that parameter. The parameters were varied according to table 2.

Table 2 Parameter variation values

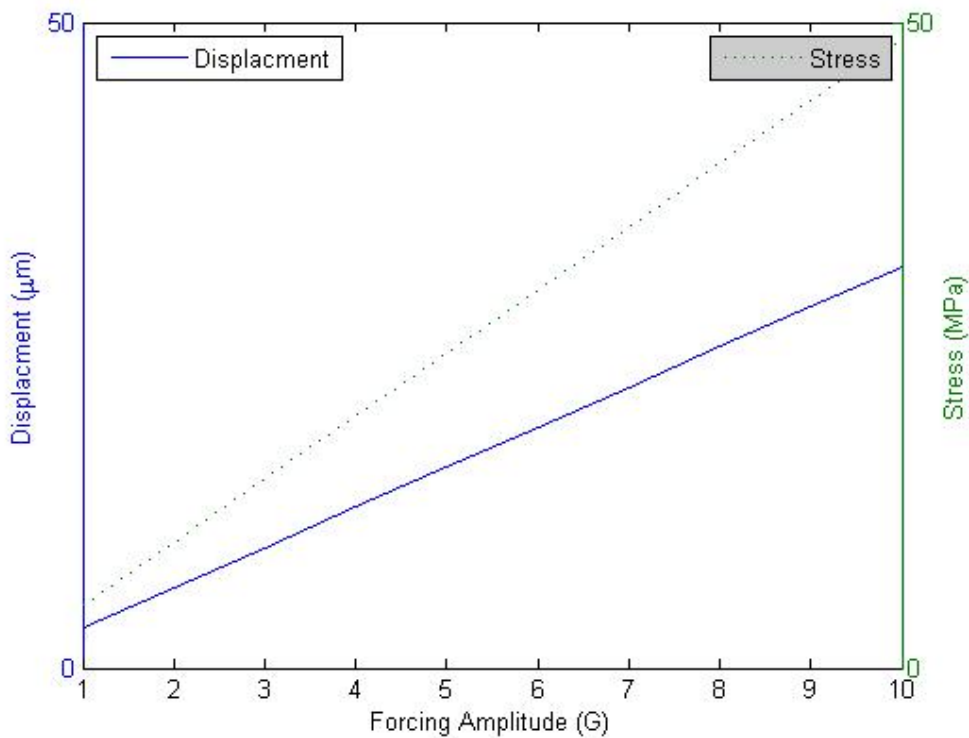| Parameter	Minimum	Maximum	Increment
Forcing (G)	1	10	1
Frequency (Hz)	100	10,000	100
Diameter (μm)	1	10	1
Length (μm)	100	10,000	100

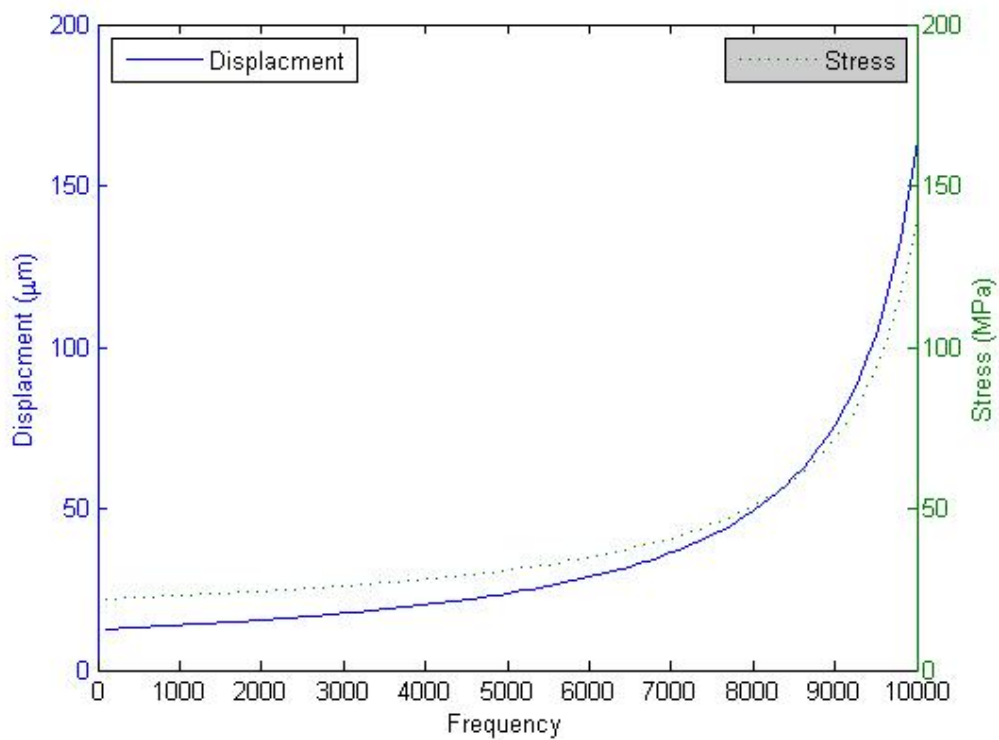**Figure 7 Forcing amplitude dependence of displacement and stress**

Figure 8 Frequency dependence of displacement and stress

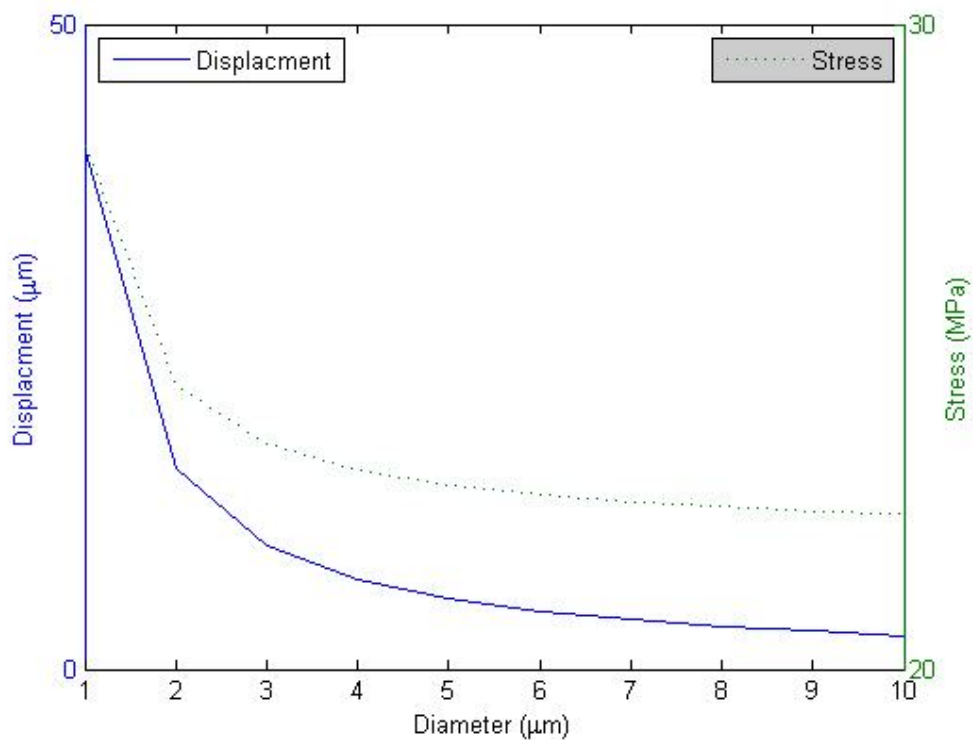**Figure 9 Whisker diameter dependence of displacement and stress**
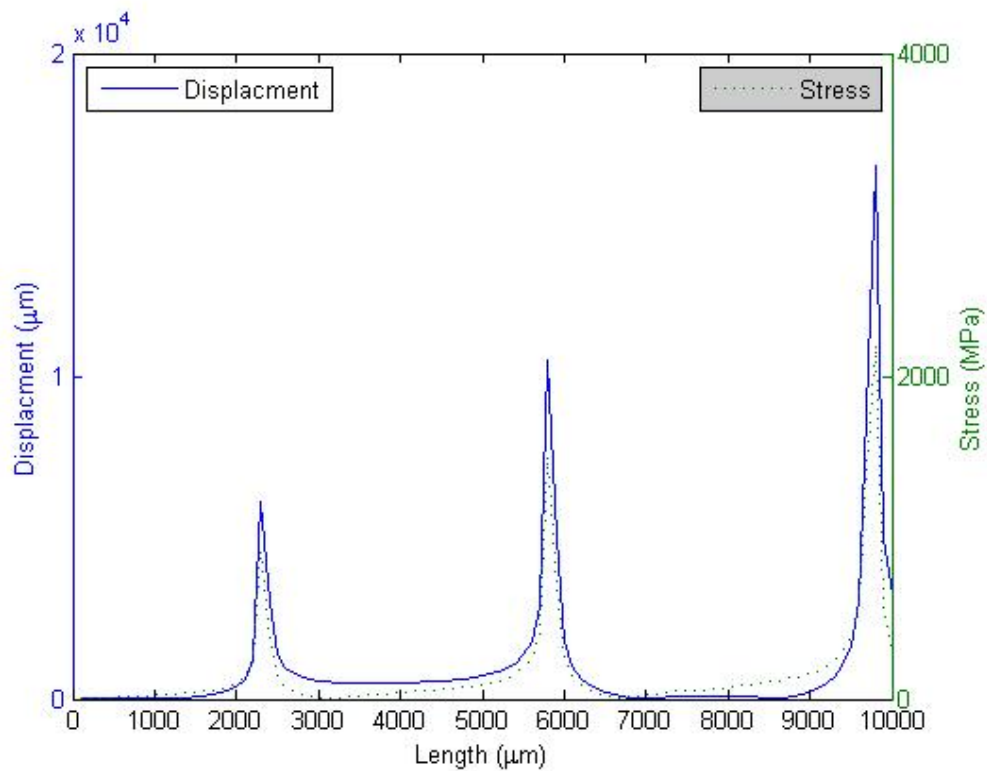

Figure 10 Whisker length dependence of displacement and stress

To give a better overall view of the response of typical whisker lengths and diameters to 5G sinusoidal forcing at 2000 Hz, both diameters and lengths were varied and plotted.
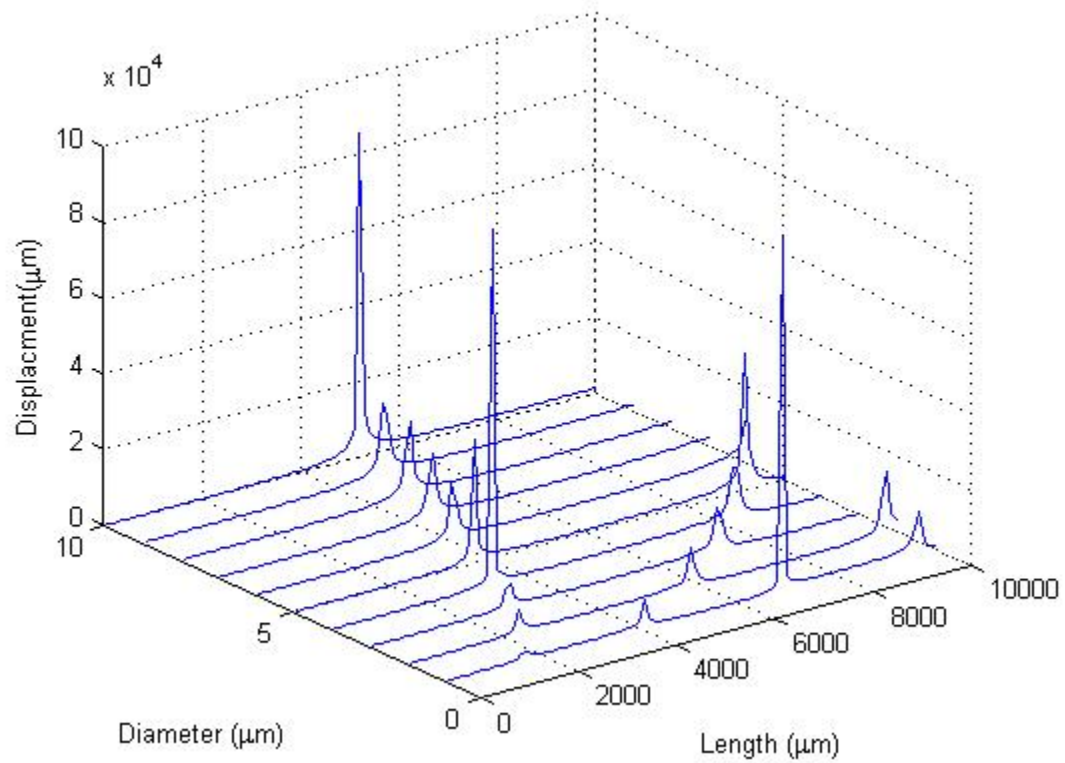

Figure 11 Peak displacement response across a wide rage of diameters and lengths
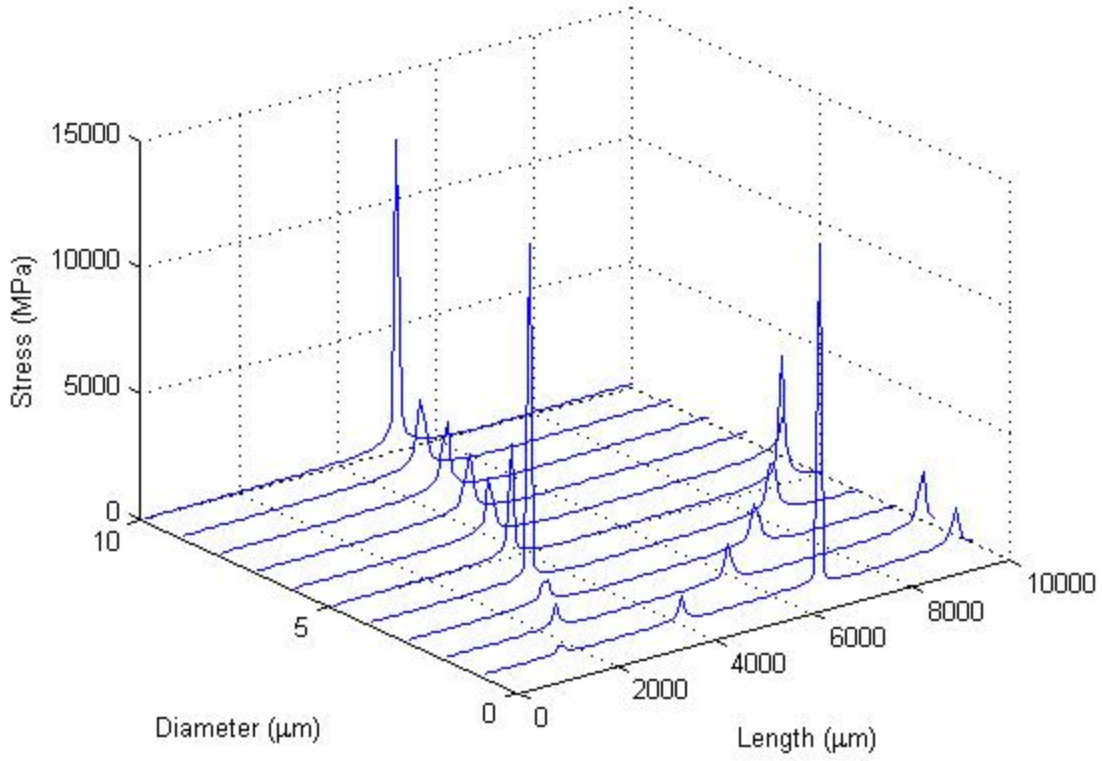
Figure 12 Stress response across a wide rage of diameters and lengths

2.5   Discussion

2.5.1   Model

To verify the numerical outputs the governing equation was non dimensionalized. The coefficients were then collected to give a non-dimensional scaling factor for comparison. The following non dimensional parameters were established,

$$\chi = \frac{x}{l} \qquad \tau = \frac{t}{l^2}\sqrt{\frac{EI}{\rho A}} \qquad \upsilon = \frac{u}{B}, \qquad (36, 37, 38)$$

and substituted into equation 2. Again neglecting tension in the beam yielded,

$$B\left[\frac{\partial^2 \upsilon}{\partial \tau^2} + \frac{\partial^4 \upsilon}{\partial \chi^4}\right] = l^4 \frac{\rho A}{EI} F(\chi, \tau). \qquad (39)$$

B was chosen as,

$$B = l^4 \frac{\rho A}{EI} = \frac{l^4}{d^2} \frac{16\rho}{E}. \tag{40}$$

Equation 40 was substituted into equation 38 which yielded,

$$u = \frac{l^4}{d^2} \frac{16\rho}{E} \upsilon. \tag{41}$$

Now the relation between the dimensional displacement and the non dimensional parameters length and diameter were compared. With a 5 G sinusoidal forcing at 2000 Hz the forms of the numerical outputs and the non dimensional parameters were plotted to assure the model was behaving as expected.
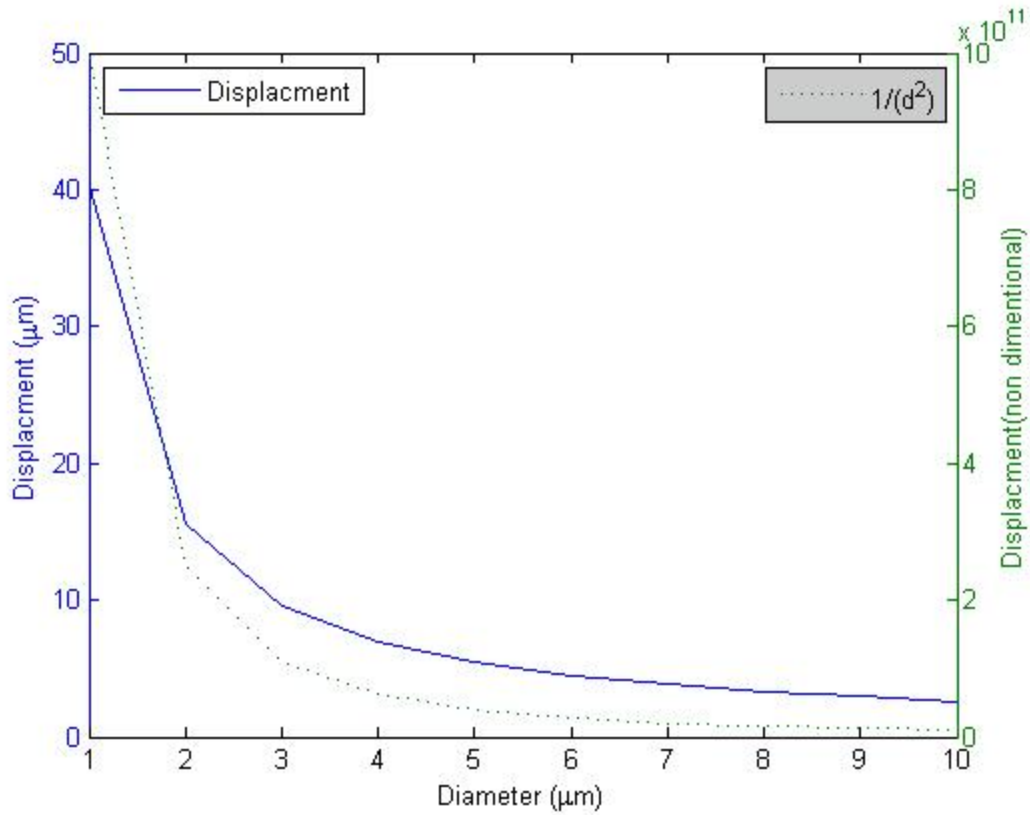

Figure 13 Comparison of diameter dependence to nondimensional parameter
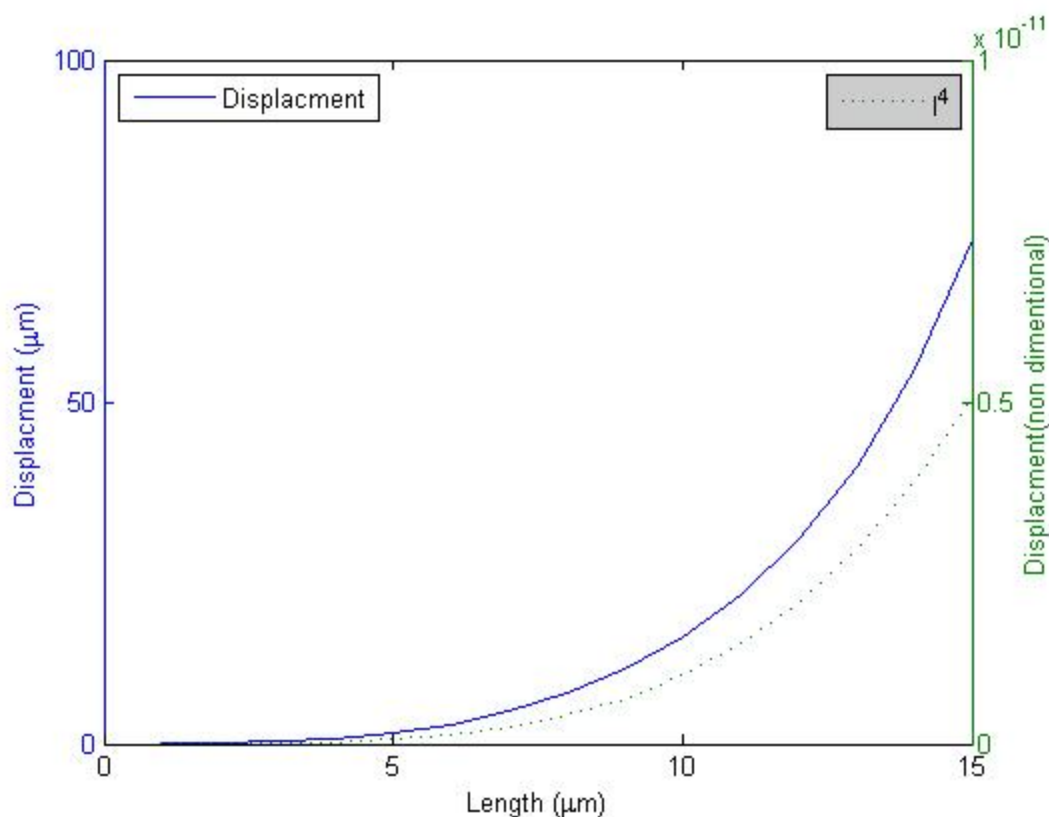
Figure 14 Comparison of length dependence to nondimensional parameter

Since the basic relationships of the non dimensional parameter held true to the numerical outputs the model was verified.

2.5.2   Parameter Variation

Figure 11 and 12 were plotted to get a broad picture of the response of tin whiskers to the highest typical forcing they will experience. The x-axis covers the range of whisker lengths reported from 0 to 10,000 μm (10 mm). The y-axis covers the range of whisker diameters reported from 1 to 10 μm. The first row of peaks represents the first resonant mode in response to the 5G 2000 Hz forcing.   The amplitude of the peaks is a function how close the discrete length plotted falls to the natural frequency and should not be considered important. The second row of peaks represents the second mode response. The value of these two plots is they quickly show the length and width combinations where tin whiskers will start to resonance and be subject to greater resulting stresses.

3. Tin Whisker Property Measurement

3.1 Introduction

Whisker properties such as yield and ultimate strength are critical to the accuracy in the analysis of whisker dynamics. A literature survey was preformed to determine if there were other studies of tin whisker properties. The vast majority of literature on tin whiskers relates to the growth mechanism, but one source was discovered where an attempt to measure tin whisker properties was made. Dunn [19] in 1988 harvested whiskers approximately 0.5 mm long and embedded them in a mound of either epoxy or indium solder on glass microscope slides. Then 40 μm diameter gold wire was cut into known lengths and formed into a hook on one end then hung onto the cantilevered whiskers. The optically measured displacement was used along with the weight of the wire to calculate modulus of elasticity. Tensile strength was measured in a similar way using a gold wire hook on one end to anchor the whisker, and another on the other end to add additional wire lengths as weights.

Modern measurement method such as Atomic Force Microscopy (AFM) and Mictotribology offers a much more precise and repeatable way to measure micro and nano structures.

3.2 Experimental Design

The experimental design was to bend a tin whisker to the point of fracture and to measure the load. The data would then be used to calculate the yield and ultimate strength. The substrates with whisker growths were surveyed for typical whisker geometries present. The longest whiskers surveyed were around 100 μm long with diameters of 4-6 μm. Rough order of magnitude calculations using the ultimate tensile strength of beta phase tin show the force required to break whiskers of this length would be expected in the range of 1000-3000 nN. Since the AFM has a typical capacity of 200 nN it is not capable of performing the experiment. The microtribometer on the other hand is capable up to 200 mN so the force required is very low in its working range. Considering the structure of the whisker to be a very pure single crystal free of most impurities or defects it is logical to assume the strength is likely to be higher than that of a macro sized sample used for typical tensile tests.

The microtribometer used was custom built by Iowa State University based on Bhushan and colleagues and a schematic of the major components can be seen in reference 20. The basic design an armature composed of crossed I beams with semiconductor strain gages. Custom designed probe tips can be bonded to a small screw and attached to the armature with a nut. For the whisker test a thin rigid probe tip was desired. A stainless steel blade was bonded to a hex head bolt with high strength epoxy adhesive as seen in figure 15.
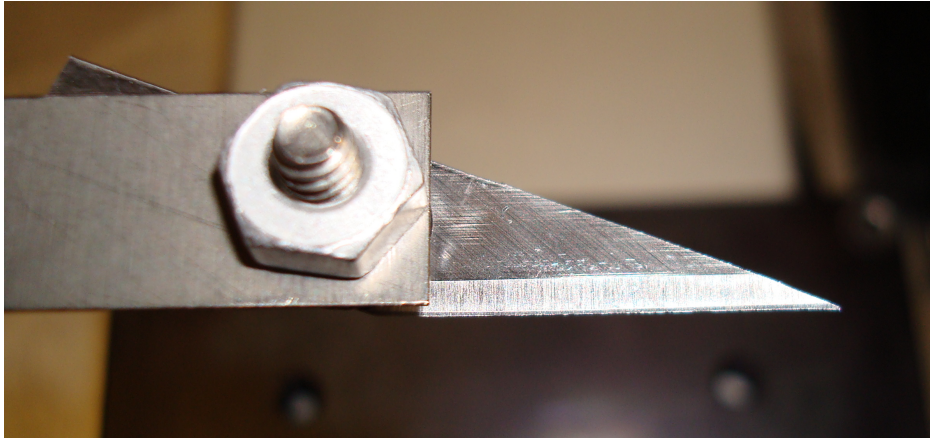

Figure 15 Stainless steel blade used for probe tip

The armature was attached to a vertical actuation stage for positioning the tip relative to the height of the whisker. The sample was placed on a horizontal stage perpendicular to the armature. This stage was used to bring the tip in contact with the whisker and perform the test. A stereomicroscope was used from the vertical position to roughly align the probe tip and the sample. Another microscope hooked up to a digital camera and computer was used to align the tip to the whisker. The focal plane was used to make depth of field refinements to the initial alignment provided by the stereomicroscope. This microscope also preformed the image capture. A picture of the setup can be seen in figure 16.
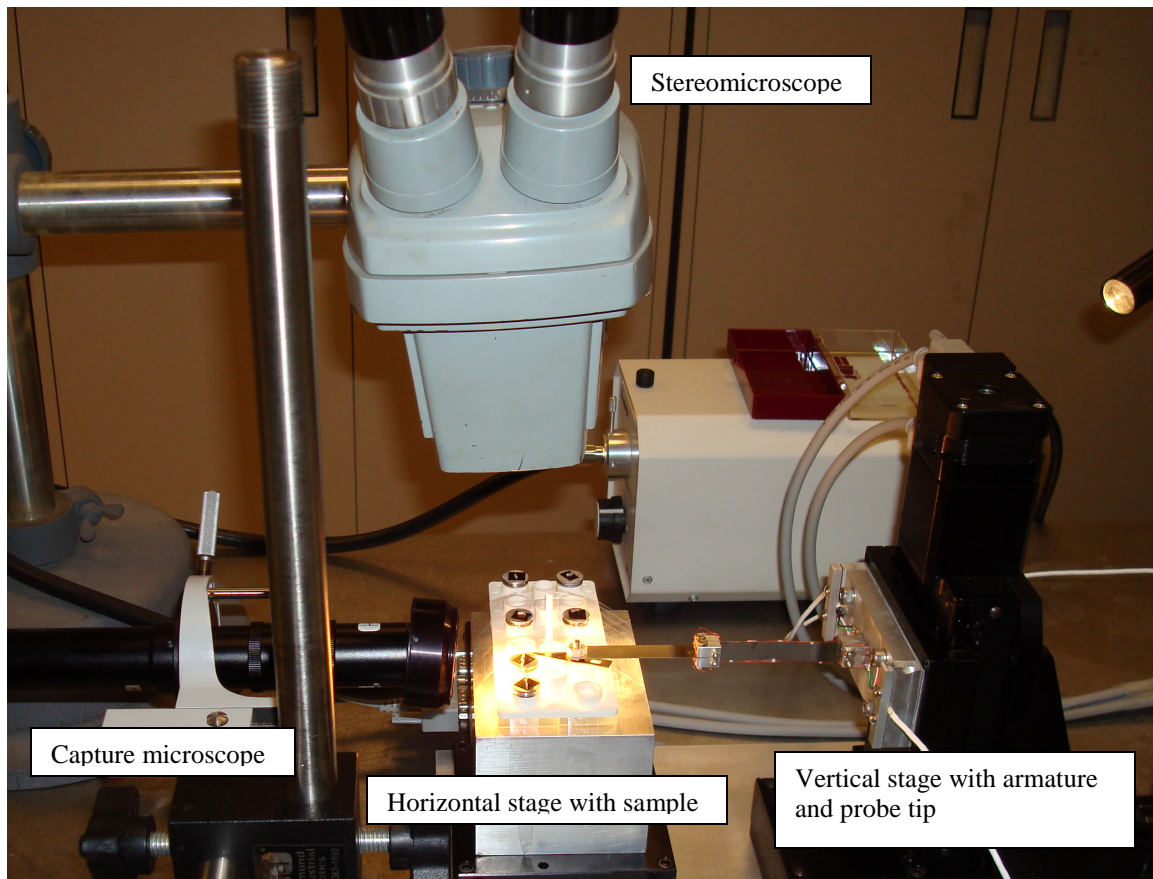
Figure 16 Experimental setup

3.3   Sample Preparation

Whisker samples were prepared from test boards that have undergone unrelated testing. The boards each had 12 or more dual inline package (DIP) integrated circuits (IC) with tin plated lead frames. The tin plating on the lead frames had begun growing whiskers, and by surveying the boards solitary whiskers of significant length were identified. The identified leads were clipped from the board and affixed to a scanning electron microscope (SEM) mount using carbon tape. The whiskers were oriented vertically for optimum use in the experimental setup. The mounts were then placed in the SEM for measurement. The full set of SEM images can be seen in appendix B, and one is presented here for reference. At 30 times magnification the whisker is just barely visible. At 800 times magnification the whisker's form (straight with a slight curl on the tip), and the striations running the length of the body are visible. The whisker length is 109.5 μm and diameter is 6.86 μm.
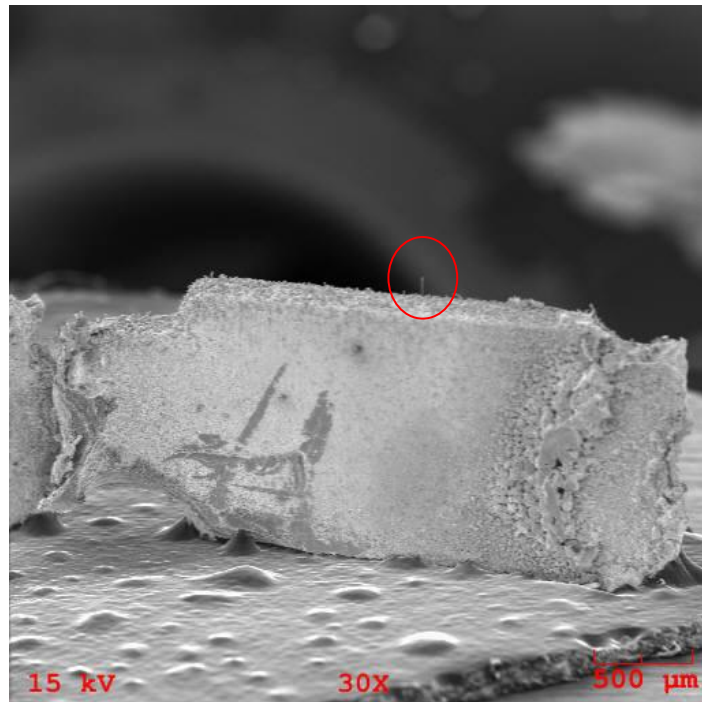
Figure 17 30x magnification of whisker on edge of lead
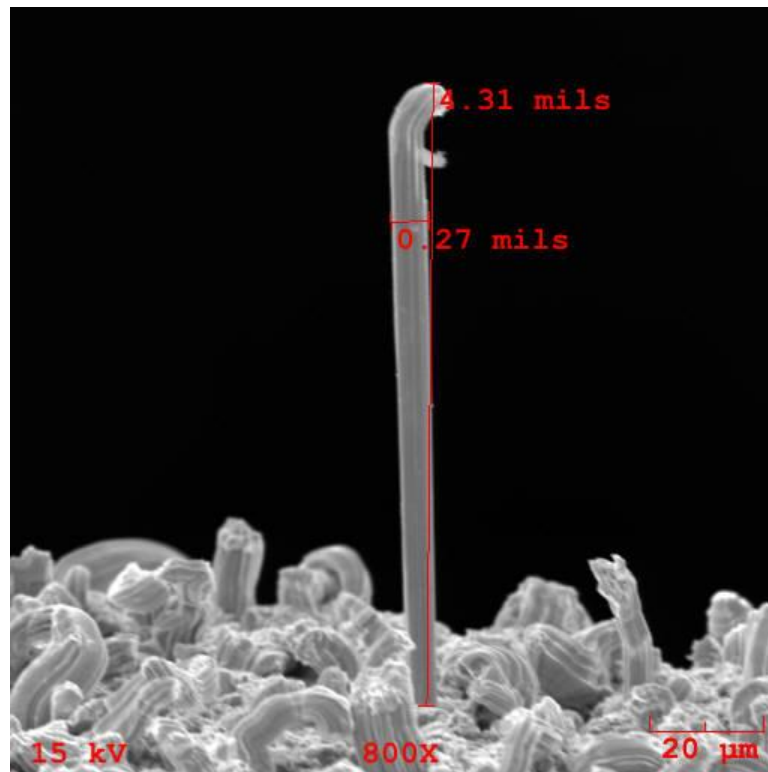

Figure 18 800x magnification of whisker

3.4   Results

The method used to perform the test was to align the probe tip relatively low on the whisker without touching the substrate surface. The reason for seeking a low contact point was to reduce the lever arm and increase the forces required to break the whisker making the measurement easier to resolve. The normal force of the probe was monitored to assure no contact was made with the substrate. The sample was then moved toward the probe in 2 μm increments until the probe had passed over the whisker entirely. Figure 19 presents a sequence of image captures representing the test process.

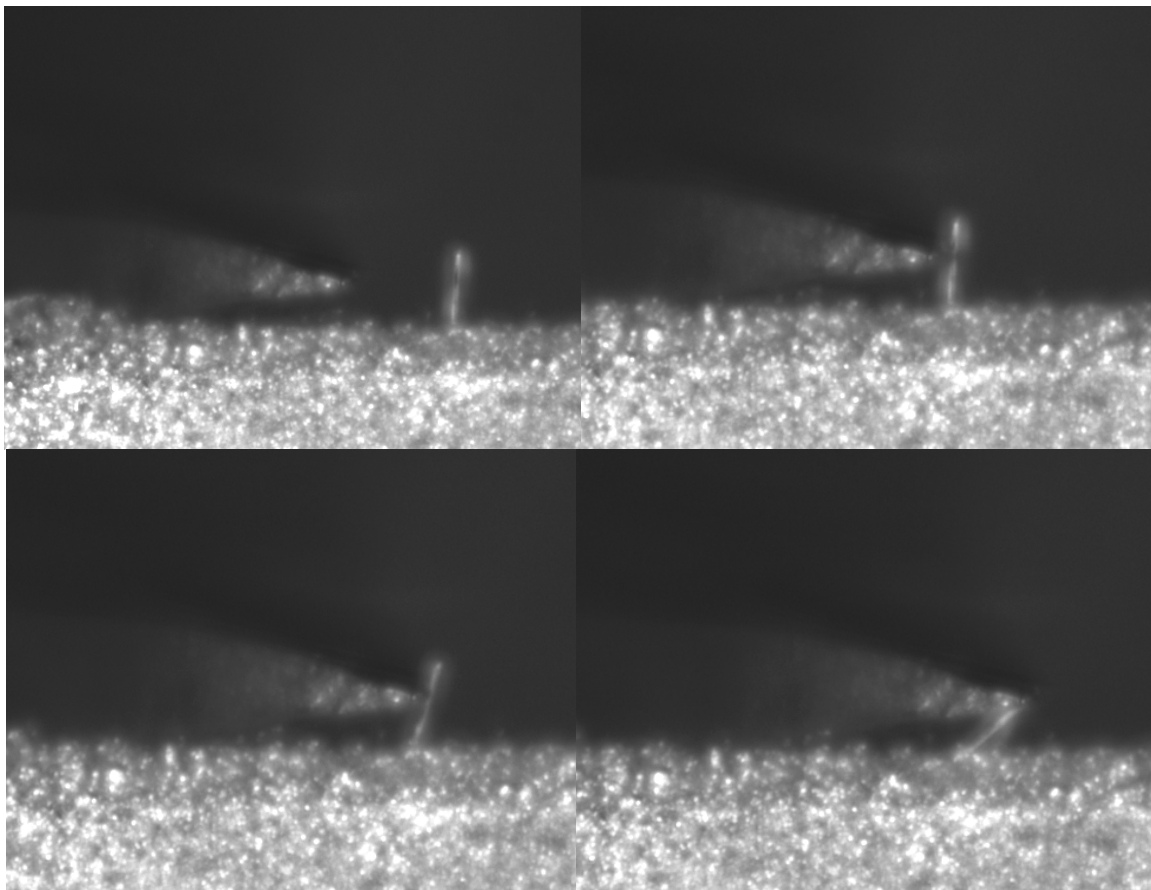**Figure 19 Incremental steps of whisker test on whisker sample 3**

Both the normal and tangential forces were recorded throughout the test. The tangential force was measured relative to the direction of motion, meaning an increasing tangential force was plotted as an increasing negative number. The raw data is presented along with a plot of the moving average to filter out some of the noise.
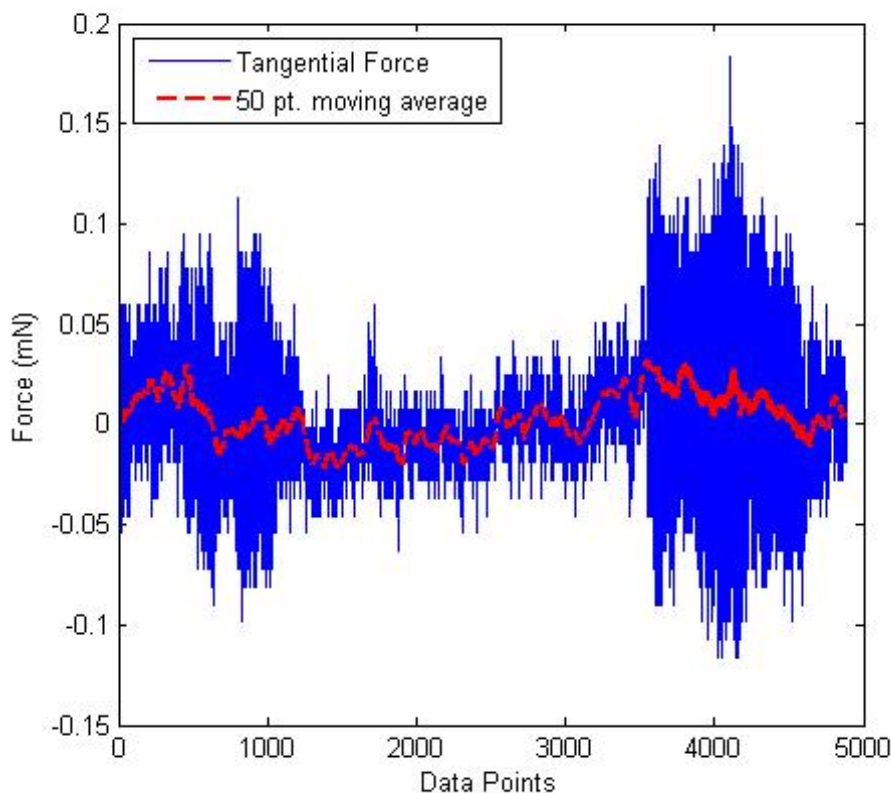
Figure 20 Tangential force, whisker sample 3

The two larger "noisy" lobes on the left and right represent time the probe was not in contact with the whisker. The tighter band in the center represents the time the probe was in contact and deforming the whisker. The noise seen in the data when the probe is not in contact with the whisker is probe oscillation due to acoustic vibration or structural vibration not filtered by the table. The peak tangential force measured during whisker contact was 21.8 μN.

Since whisker sample 3 presented did not break off a secondary method was employed to see if the force could be measured while the whisker broke. The sample was reset as before but this time the probe was brought down and placed in contact with the substrate with a minimal amount of normal force. The sample was then moved toward the probe again at 2 μm increments until the whisker had moved completely past the probe. In this case the tangential force is actually the frictional force.

Figure 21 Frictional force, whisker sample 3

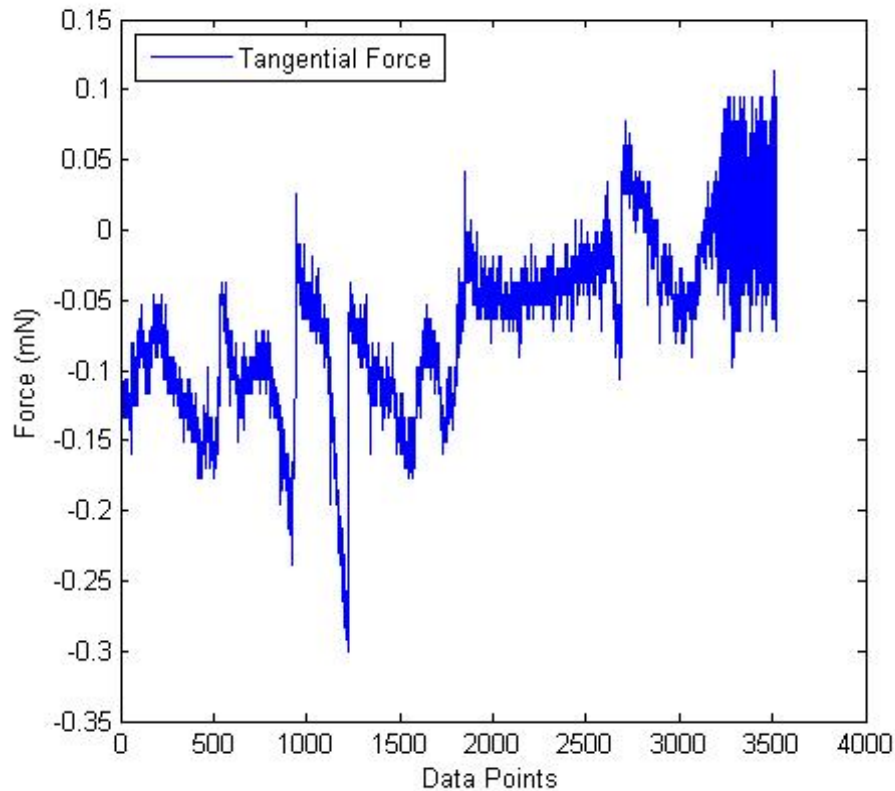It should be noted that when the probe tip is in contact with the substrate it is stabilized and the data is not as noisy, and does not require a moving average. The data from 0 to the vertical jump just before 1000 was the friction force with the substrate. Data from 1000 to approximately 3000 was the contact with the whisker. After 3000 the probe lost contact with the substrate and the noisy oscillations can be seen again as in figure 20. To calculate the frictional force attributed to the whisker the frictional force prior to contact must be calculated and removed from the portion of the data where the probe was also in contact with the whisker. Using this method the frictional force attributed to the whisker alone was 187.2 μN. This was more than measured previously, but contact point was also much lower to the base which would lead to an increased force. Although this method seemed to work reasonably well it was abandoned due difficulties with plating irregularities and questions about test isolation between the target whiskers and other shorter surrounding whiskers.

The remaining whiskers were tested with the non contact tangential force measurement method. The first 3 samples were tested at 2 μm increments, and the remaining 4 samples were tested with a linear pass of 250 μm at a rate of 1000 μm per second. By running the test with a short linear sweep less noise was introduced into the data. As seen in figure 22 the spike in tangential force is much clearer.
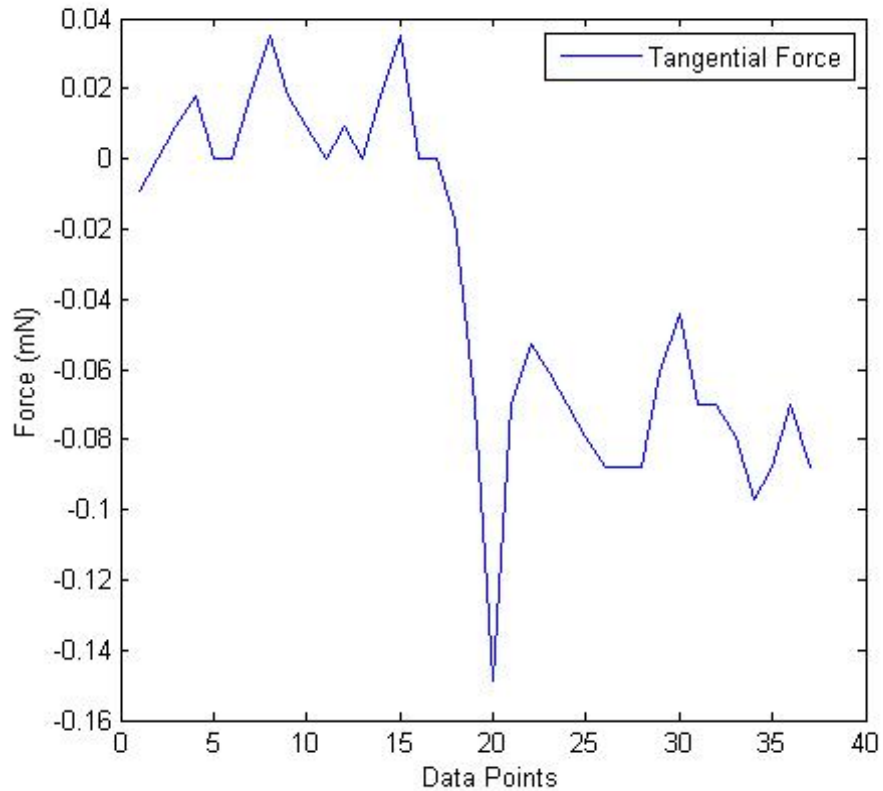

Figure 22 Tangential force, whisker sample 5

Once the peak tangential forces were found for each sample whisker the bending stress was calculated based on the geometry using static beam equations. A summary of the sample geometries, peak tangential forces, and calculated stresses is presented in table 3. Complete sample image, and force data is presented in appendix C.

Table 3 Summary of whisker geometry, peak force, and stress

Sample	L (μm)	Contact Height (%)	d (μm)	Peak Force (μN)	Deformation Stress (MPa)
1	69.8	55	5.3	73	192
2	78.9	58	4.5	51	252
3	109.4	57	6.8	21	43
3$_{sliding}$	109.4	26	6.8	187	168
4	77.4	58	8.3	33	26
5	92.4	73	5.0	149	778
6	52.8	64	8.3	1059	617
7	55.8	53	8.8	279	120

3.5   Discussion

The first observation in the testing was that the whiskers did not break off as expected. Since they are single crystal grows it was expected that the structure would be brittle and fracture when excessive force was applied. Instead the structure yielded plastically. Within the resolution of the capture microscope no spring back was noted with any whisker. However it is clear from the capture images that the bulk of the whisker body remained straight throughout the testing. This leads to one of two conclusions: that the very root of the whisker was yielding where the bending moment was the greatest or the surrounding grain structure where the whisker grew was yielding. The samples have been sent back to the lab to try to determine from SEM imaging which is the case.

Looking at the data for the one test done with the sliding method it is apparent that there was stick-slip behavior where the tangential force would build up then suddenly the probe tip would release and the tangential force would jump down before building again. This happened several times on the substrate leading up to the whisker and even on the whisker itself once the yielded angle allowed the probe to begin sliding over the whisker. These slips could be from normal friction, but they could also be from other small whiskers or plating nodules. The data supports previously stated concerns that the sliding method should be avoided due to uncertainly with the testing conditions and this data was discarded.

The data for the incremental step tests (sample 1-3) did show a rise in tangential force when in contact with the whisker, but this rise was quite small in contrast to the noise present in the data. The fact that a moving average was needed to filter out the noise leads to concerns about the validity of the data. For this reason the first three samples measured with the incremental steps was discarded.

The remaining samples that were tested in one smooth motion exhibited a clear rise in tangential force while in contact with the whisker and a drop once the probe tip had passed over the whisker. Sample 4 did exhibit noise and force measurements that were similar in magnitude and for this reason was discarded. The remaining samples 5, 6 and 7 all showed some noise, but it was low relative to the peak force measured. This noise was most likely due to acoustic vibrations or slight slipping on the whisker as force was applied. The higher point of force application precluded any questions about interference from short surrounding whiskers. Examination of the normal forces of sample 6 and 7 show effectively no normal force before and after contact whisker contact with an increased measurement when applying force to the whisker. This validates that the probe only came in contact with the subject whisker. Sample 5 showed similar measurements but had a residual normal and tangential force after force application. This was due to the probe not traveling far enough to entirely pass over the whisker. The whisker remained in contact with the underside of the probe causing the residual forces.

When examining the peak forces measured they were all on the order of 1 mN or less. For a device that is design to measure up to 200 mN this is extremely low in the working range. Error from acoustic or structural vibration could greatly influence the results. Looking at the calculated stress results is it hard to know if the great variability (ranging from 120 to 778 MPa) was due to introduction of error or to whisker variability. To resolve this question the working range of the microtribometer must be lowered to something more appropriate for the expected values, and error sources such as acoustic vibration must be better controlled. This is normally done with an enclosure over the test set up but the required microscope equipment prevented its use for this test.

Another factor to consider when looking at the variability of the measurements is the crystal orientation. Since tin whisker crystals are know to grow in a variety of directions, the

orientation could have a large impact on the force required to deform the whisker. Looking at sample 6 and 7 it can be seen that their diameter is nearly the same but their deformation stress was an order of magnitude different. Crystal orientation could be a factor in this difference.

Ignoring the sources of variability and examining the deformations stresses of the three valid measurements, it is noted that two of them are above 220 MPa, the ultimate tensile strength of bulk tin, and one is lower. These values were compared to the plots of section 2.4.2. It was clear that under the typical loading whiskers less than 2mm in length would not resonate in response to forcing at 2000 Hz, and would not experience stresses greater than measured in the experiment. Smaller whiskers simply are too light and too stiff for inertial loading typically seen in electronics to cause deformation. Only whiskers of length greater than 2 mm (and longer at larger diameters) would see resonance and stresses large enough to cause deformation. Only the combination of very long whiskers, small diameters and heavy loading is likely to cause a whisker break due to inertial loading.

4. Future work

4.1 Modeling

Although reported typical values for tin whiskers were on the order of 1mm length and 1-4 μm diameters, the whiskers found on the samples prepared for property analysis were much shorter and somewhat thicker. Given the approximate length of 100 μm and a diameter of 4-6 μm the slenderness ratio of the samples was 16-25. This was far less that the threshold of 100 used to validate the selection of the Euler-Bernoulli model. If analysis of short whiskers, on the order of 500μm or less, is desired in the future the Timoshenko model should be considered to increase accuracy.

Additional input types should be added such as shock loading and random vibration. Since eigenfunction expansion is already being used it is a natural extension to use a Fouier series to represent a shock loading, and the forcing function in the model. For random vibration there are methods of casting the equation of motion for principle coordinates into the frequency domain and then solving for mean square values of the displacement. This method is straight forward and should be adaptable to the eigenfunction expansion problem.

4.2 Measurements

There are many additional avenues of research that would aid in the development of a more accurate risk assessment model. First and fore most would be the refinement of the forces and stresses developed in this experiment. With a basis of design a microtribometer arm of appropriate dimensions and strain gauges could be developed that would allow more accurate measurement of the whiskers. Another important factor to consider is the crystal orientation. This crystal orientation should be measured prior to force application and deformation measurements to determine if there is a directional dependence. These two factors should be combined with an increase in sample size to give a better statistical measurement base.

Dampening present in the whiskers would be another important issue especially in longer whiskers that would experience resonance. Without dampening ratio the model becomes very inaccurate near resonance as the displacement amplitude climbs without

bound. Fatigue stress could also be studied to aid in the development of a risk model. Vibration levels may not be enough to deform whiskers under low cycle stress but prolonged exposure are certain amplitudes could lead to high cycle fatigue life failures and greater potential risk.

References

[1]. Brusse, J., G. Ewell, and J. Siplon, "Tin Whiskers: Attributes and Mitigation", Capacitor and Resistor Technology Symposium (CARTS) Europe, October 15-17, 2002, pp.221-233.

[2]. Brusse, J., H. Leidecker, L. Panashchenko, "Metal Whiskers: Failure Modes and Mitigation Strategies", Second International Symposium on Tin Whiskers, Toyko, Japan, April 24, 2008.

[3]. Brusse, J. "Tin Whiskers: Revisiting an old problem", NASA's EEE Links Newsletter, December 1998.

[4]. Sampson, M., H. Leidecker, J. Kadesch, J. Brusse, "Basic Information Regarding Tin Whiskers," NASA Goddard Tin Whisker Homepage, Febuary 22, 2007, http://nepp.nasa.gov/whisker/background/index.htm, accessed April 9th, 2009.

[5]. Fontana, P. "SEM images of a 27 year old sample containing tin whiskers in comparison to salt (NaCl) whiskers," NASA Goddard Tin Whisker Homepage, June 2008, http://nepp.nasa.gov/whisker/reference/reference.html, accessed April 9th, 2009.

[6]. Dunn, B., "A Laboratory Study of Tin Whisker Growth," European Space Agency STR-223, September 1987.

[7]. Woodrow, T., "Tracer Diffusion is Whisker Prone Platings," SMTA International Conference, September 2006.

[8]. Timoshenko, S., History of Strength of Materials, New York: Dover Publications, Inc.1953.

[9]. Han, S. M., H. Benaroya, T. Wei, "Dynamics of Traversely Vibrating Beams using four Engineering Methods," Journal of Sound and Vibration, 1999.

[10]. Timoshenko, S., "On the correction for shear of the differential equation for transverse vibrations of bars of uniform cross-section," Philosophical Magazine, 744, 1921.

[11]. Timoshenko, S., "On the transverse vibrations of bars of uniform cross-section," Philosophical Magazine, 125, 1922.

[12]. Egle, D., "An approximate theory for traverse shear deformation and rotary inertia effects in vibrating beams," Clearinghouse for Federal Scientific and Technical Information, May 1969.

[13]. Mirovitch L., Elements of Vibration Analysis, Mc Graw Hill, 1975.

[14]. Rao, S., Mechanical Vibrations 4th ed., Pearson Education, 2004.

[15]. Farlow, S., Partial Differential Equations for Scientists and Engineers, Dover Publications, 1993

[16]. MIL-STD-810F, "Environmental Engineering Considerations and Laboratory Tests," January 1st, 2000.

[17]. Carlson, A., P. Crilly, J., Rutledge, Communication Systems, Mc Graw Hill, 2002.

[18]. Lathi, B., Linear Systems and Signals 2nd Ed., Oxford University Press, 2005.

[19]. Dunn, B., "Mechanical and Electrical Characteristics of Tin Whiskers with Special Reference to Spacecraft Systems," European Space Agency Journal, January 14, 1988

[20]. Check, J., K. Karuppiah, S. Sundararajan, "Comparison of the effect of surface roughness on the micro/nanotribological properties of ultra-high-molecular-weight polyethylene in air and bovine serum solution," Wiley Interscience, July 18, 2005. PDEs for engineers and scientists

Appendix A   Matlab Code

```matlab
clear;


%-------------------------------------------------------------------------
%Global loop2 for parameter variation
zz=1;                   %initialize global loop index
%for gll=1:1:10;          %global loop



%-------------------------------------------------------------------------
%Global loop for parameter variation
z=1;                    %initialize global loop index
%for gl=1:1:10;          %global loop



%-------------------------------------------------------------------------
%Variables used in calculations
n=1;                    %indexing variable
x=sym('x');             %define x as a symbolic variable for integration
t=sym('t');             %define t as a symbolic variable for integration
T=sym('T');             %define T as a symbolic variable for integration



%-------------------------------------------------------------------------
%Resolution Parameters of problem
maxev=15;               %maximum number of eignevalues to find
%maxev=gl;              %maximum number of eignevalues to cycle in  global
loop
res=0.001;              %resolution to calculate eigenvalues (low
resolution, refined later)
ts=100;                 %number of time steps

format short



%-------------------------------------------------------------------------
%User Defined Parameters
d=2e-6;                 %whisker diameter
%d=1e-6*gl;             %whisker diameter - Global Loop

l=1000e-6;              %whisker length
%l=100e-6*gl;           %whisker length - Global loop

p=5765;                 %whisker density
E=220e9;                %whisker modulus


%Ipos=(.05*l)*x;        %initial deflection
%Ivel=(.05*l)*x;        %initial velocity
Ipos=0;                 %initial deflection from rest
```

```
Ivel=0;                     %initial velocity
G=5;                        %Gs level form vibration test
%G=gl*1;                     %Gs level - Global loop

omega=2000;             %forcing frequency
%omega=100*gl;            %forcing frequency - Global loop


%-------------------------------------------------------------------------
%Derived  Parameters

r=d/2;                  %whisker radius
A=3.14*(r^2);           %whisker crossectional area
I=((d^4)*(pi))/64;      %whisker moment of inertia
m=(A*l)*p;              %whisker mass
c=((E*I)/(p*A))^0.5;    %combination constant

g=9.80665;              %standard gravity
a=G*g;                  %acceleration
F=(m*a)/l;              %Force per meter applied force
force=F*sin(omega*t);   %forcing function

tres=1/(2.1*omega);     %time resolution
tmax=ts*tres;           %time maximum

%-------------------------------------------------------------------------
%plot of the frequency equation

n=1;
for k=0:res:100;
y(n)=(cos(k)*cosh(k))+1;
n=n+1;
end

%-------------------------------------------------------------------------
%looks for values of zero indicating an eigenvalue (low resolution)

k=0:res:90;                     %sets range to look for eigenvalues
counter=1;                      %defines a counter varable to count how many
                                 eigenvalues have been found
bl=zeros(1,maxev);              %defines a matrix to store the eigenvalues
thresh = 0;                     %defines the trigger point

for i=1:length(y)-1
    if counter<=maxev
        if(y(i+1)>thresh & y(i)<=thresh)
            bl(counter)=k(i);
            counter=counter+1;
        elseif (y(i+1)<thresh & y(i)>=thresh)
            bl(counter)=k(i);
            counter=counter+1;
        end
    end
end
```

```matlab
%------------------------------------------------------------------------
%Takes low resolution eigenvalues and uses them for an initial guess in
the fzero function to find eigen values to the full double floating point
resolution

for i=1:1:maxev;
bl(i)=fzero('cos(x)*cosh(x)+1',bl(i));
end

n=1;
for k=0:res:90;
v(n)=(cos(k)*cosh(k)+1);
n=n+1;
end



%------------------------------------------------------------------------
%beta only component of the eigenvalues (bl)

b=bl/l;

%------------------------------------------------------------------------
%natural frequencies associated with eiganvalues in hertz

w=((bl.^2)*(((E*I)/(p*A*(l^4)))^.5));

%------------------------------------------------------------------------
%Eigenfunctions associated with eiganvalues (bl)

for i=1:1:maxev;                  %indexing cycle (1 through max number of
                                    eigenvalues)
efunction(i)=((sin(b(i)*x))-(sinh(b(i)*x)))-
((((sin(bl(i)))+(sinh(bl(i))))/((cos(bl(i)))+(cosh(bl(i)))))*((cos(b(i)*x)
)-(cosh(b(i)*x))));
end

for i=1:1:maxev;        %loops eigenvalues for the next 3 sections
%------------------------------------------------------------------------
%Equation of generalized force

integrand1(i)=force*efunction(i);   %integrand of generalized force
                                     (forcing x eiganvenctor)
Q(i)=((int(integrand1(i),x,0,l)));   %generalized force



%------------------------------------------------------------------------
%Calculates the transformed initial position values

integrand2(i)=efunction(i)*Ipos;        %integrand of initial position
                                         Coeficient
IposC(i)=eval(int(integrand2(i),x,0,l));    %Initial position coefficient
```

```matlab
%-------------------------------------------------------------------
%Calculates the transformed initial velocity values

integrand3(i)=efunction(i)*Ivel;        %integrand of initial velocity
                                         Coefficient
IvelC(i)=eval(int(integrand3(i),x,0,l));    %Initial velocity coefficient

end


%-------------------------------------------------------------------
%Calculation of An

for i=1:1:maxev         %cycles through the eigenvalues
An(i)=IposC(i)-((1./(w(i)-omega))*(1/(p*A))*(Q(i)));
end


%-------------------------------------------------------------------
%Calculation of Bn

for i=1:1:maxev         %cycles through the eigenvalues
Bn(i)=(1./w(i))*(IvelC(i)-(diff(((1./(w(i)-omega))*(1/(p*A))*(Q(i))),t)));
end


%-------------------------------------------------------------------
%Plot eigenfunctions

modeshape=zeros(maxev,100);

for i=1:1:maxev;        %cycles through the eigenvalues

n=1;
for x=0:(l/100):l;      %evals eigenfunctinos across length
modeshape(i,n)=eval(efunction(i));
n=n+1;
end

modeshapemax(i)= max((modeshape(i,:)));
end

%for i=1:1:maxval;       %Normalizes eigenfunctinos
%modeshape(i,:)=modeshape(i,:)/modeshapemax(i);
%end

%figure(1);             %Plots mode shapes
%x=0:(l/100):l;                          %Cylces though time domaine
%plot(x,modeshape(:,:));                 %Plot tip deflection vs time
%%axis([0 20 -1e-23 1e-23]);             %plot axis control
```

```matlab
%grid;                                   %add a grid
%ylabel('Length (m)');
%xlabel('displacment');
%title('Mode Shapes');


%-------------------------------------------------------------------
%Eval of An

t=0;
for i=1:1:maxev;            %cycles through the eigenvalues
AnE(i)=eval(An(i));
end

%-------------------------------------------------------------------
%Eval of Bn

t=0;
for i=1:1:maxev;            %cycles through the eigenvalues
BnE(i)=eval(Bn(i));
end

%-------------------------------------------------------------------
%Calculation of the generalized coordinate

for i=1:1:maxev            %cycles through the eigenvalues
q(i)=((AnE(i)*cos(w(i)*t))+(BnE(i)*sin(w(i)*t))+((1/(w(i)-
omega))*(1/(p*A))*(Q(i)))));
end


%-------------------------------------------------------------------
%Calculation of the mode superposition solution

for i=1:1:maxev            %cycles through the eigenvalues
u(i)=efunction(i)*q(i);    %generalized coordinate * mode shapes
(eigenfunctions)
end

%-------------------------------------------------------------------
%Calculation of the bending moment

for i=1:1:maxev            %cycles through the eigenvalues
M(i)=E*I*(diff(u(i),'x',2));        %define sybolic equation for
                                    moment, based on total solution u

end


%-------------------------------------------------------------------
```

```
%Plot of whisker tip deflection vs time.

n=1;                                    %counter reset
x=l;                                     %Set x to whisker tip, maximum
deflection

for t=0:tres:tmax;                       %Cylces though time domaine
u1=eval(u);                              %evaluates total solution (u) at each
time (t), for each eigenvalue (n), and stores in u1
u2(n)=sum(u1');                          %Sums the evaluated eigenventors in u1
and stores them in u2
n=n+1;                                   %cycles though eigenvalues, for each
time step
end


%figure(2);
%t=0:tres:tmax;                          %Cylces though time domaine
%plot(t,u2);                             %Plot tip deflection vs time
%%axis([0 20 -1e-23 1e-23]);            %plot axis control
%grid;                                   %add a grid
%ylabel('Displacement (m)');
%xlabel('time (s)');
%title('Displacement at Whisker Tip');

%-------------------------------------------------------------------------
%Calculation of dynamic moment.

n=1;                                    %counter reset
x=0;                                     %Set x to whisker base, maximum moment

for t=0:tres:tmax;                       %Cylces though time domaine
M1=eval(M);                              %evaluates moment(M) at each time (t),
for each eigenvalue (n), and stores in M1
M2(n)=sum(M1');                          %Sums the evaluated moments in M1 and
stores them in M2
n=n+1;                                   %cycles though eigenvalues, for each
time step
end

%t=0:tres:tmax;                          %Cylces though time domaine
%plot(t,M2);                             %Plot moment vs time
%axis([0 20 -5e-29 5e-29]);             %plot axis control
%grid;                                    %add a grid


%-------------------------------------------------------------------------
%Calculation of dynamic bending stress at whisker root

for t=0:tres:tmax;                       %Cylces though time domaine
BS=(M2*r)/I;                             %calculate bending stress
end
```

```matlab
%figure(3);
%t=0:tres:tmax;                          %Cylces though time domaine
%plot(t,BS);                             %Plot stress vs time
%%axis([0 20 -1e-11 1e-11]);             %plot axis control
%grid;                                   %add a grid
%ylabel('Stress (Pa)');
%xlabel('time (s)');
%title('Bending Stress at Whisker Root');

%-----------------------------------------------------------------------
%Storage vectors for global loop

u2max(zz,z)=max(u2);
u2min(zz,z)=min(u2);
BSmax(zz,z)=max(BS);
BSmin(zz,z)=min(BS);
%nd(zz,z)=((l^4)*((p*A)/(E*I)));
dplot(zz,z)=1/(d^2);
z=z+1;
end

%for z=1:1:10;
%u2maxnd(zz,z)=u2max(zz,z)/nd(zz,z);
%end

%zz=zz+1;
%end

%figure(5);
%i=1:1:z-1;                              %Cylces though each global loop
%plot(i*1000,u2max);                     %Plot max tip displacment vs
global loop
%axis([0 20 -1e-11 1e-11]);             %plot axis control
%grid;                                   %add a grid
%ylabel('Displacment (m)');
%xlabel('Forcing Frequecy (Hz)');
%title('Maximum Tip Displacment vs Forcing Frequency');

%figure(6);                              %zoomed fig 5
%i=1:1:z-1;                              %Cylces though each global loop
%plot(i,u2max);                          %Plot max tip displacment vs global
loop
%axis([0 15 3.415e-5 3.43e-5]);          %plot axis control
%grid;                                   %add a grid
%ylabel('Displacment (m)');
%xlabel('Total Eigenvalues');
%title('Maximum Tip Displacment vs Number of Eigenvalues');

%figure(7);
%i=1:1:z-1;                              %Cylces though each global loop
%plot(i,BSmax);                          %Plot stress vs time
%axis([0 20 -1e-11 1e-11]);             %plot axis control
%grid;                                   %add a grid
%ylabel('Stress (Pa)');
```

```
%xlabel('Forcing Frequecy');
%title('Bending Stress vs Forcing Frequecy');

%figure(8);
%i=1:1:z-1;                                %Cylces though each global loop
%[AX,H1,H2] = plotyy(i*1,u2max/1e-6,i*1,dplot,'plot');
%set(get(AX(1),'Ylabel'),'String','Displacment (\mum)');
%set(get(AX(2),'Ylabel'),'String','Displacment(non dimentional)');
%xlabel('Diameter (\mum)');
%%title('Whisker Diameter Dependance of Displacment and Stress');
%%set(H1,'LineStyle','--')
%set(H2,'LineStyle',':')
%legend(AX(1),'Displacment',2);
%legend(AX(2),'1/(d^2)');
%legend(AX,'Displament','Stress',2);

%figure(9);
%t=0:tres:tmax;                            %Cylces though each global loop
%[AX,H1,H2] = plotyy(t*1e3,u2/1e-6,t*1e3,BS/1e6,'plot');
%%[AX,H1,H2] = plotyy(t*1e3,u2(1,:)/((1e-6)*(nd(1))),t*1e3,u2(2,:)/((1e-
6)*(nd(2))),'plot');
%set(get(AX(1),'Ylabel'),'String','Displacment (\mum)');
%set(get(AX(2),'Ylabel'),'String','Stress (MPa)');
%xlabel('Time (ms)');
%%title('Whisker Diameter Dependance of Displacment and Stress');
%%set(H1,'LineStyle','--')
%set(H2,'LineStyle',':')
%legend(AX(1),'Displacment',2);
%legend(AX(2),'Stress');
%%legend(AX,'Displament','Stress',2);


%for j=1:1:zz-1;
%for i=1:1:z-1
%d(j,i)=j;
%end
%end

%figure(9);
%for j=1:1:zz-1;                           %Cylces though each global loop2
%i=1:1:z-1;                                %Cylces though each global loop
%plot3(i*100,d(j,i),(u2max(j,i))/(1e-6));              %Plot
stress vs time
%%%axis([0 20 -1e-11 1e-11]);          %plot axis control
%grid on;                                  %add a grid
%hold on;
%ylabel('Diameter (\mum)');
%xlabel('Length (\mum)');
%zlabel('Displacment(\mum)');
%%title('Bending Stress vs Forcing Frequecy');
%end


%figure(10);
```

```
%for j=1:1:zz-1;                          %Cylces though each global loop2
%i=1:1:z-1;                               %Cylces though each global loop
%plot3(i*100,d(j,i),(BSmax(j,i))/(1e6));              %Plot
stress vs time
%%axis([0 20 -1e-11 1e-11]);         %plot axis control
%grid on;                                 %add a grid
%hold on;
%ylabel('Diameter (\mum)');
%xlabel('Length (\mum)');
%zlabel('Stress (MPa)');
%%title('Bending Stress vs Forcing Frequecy');
%%legend([ ' third mode frequency =', num2str(modes(3))]);
%end
```

Appendix B   SEM images of tin whisker samples

Sample 1
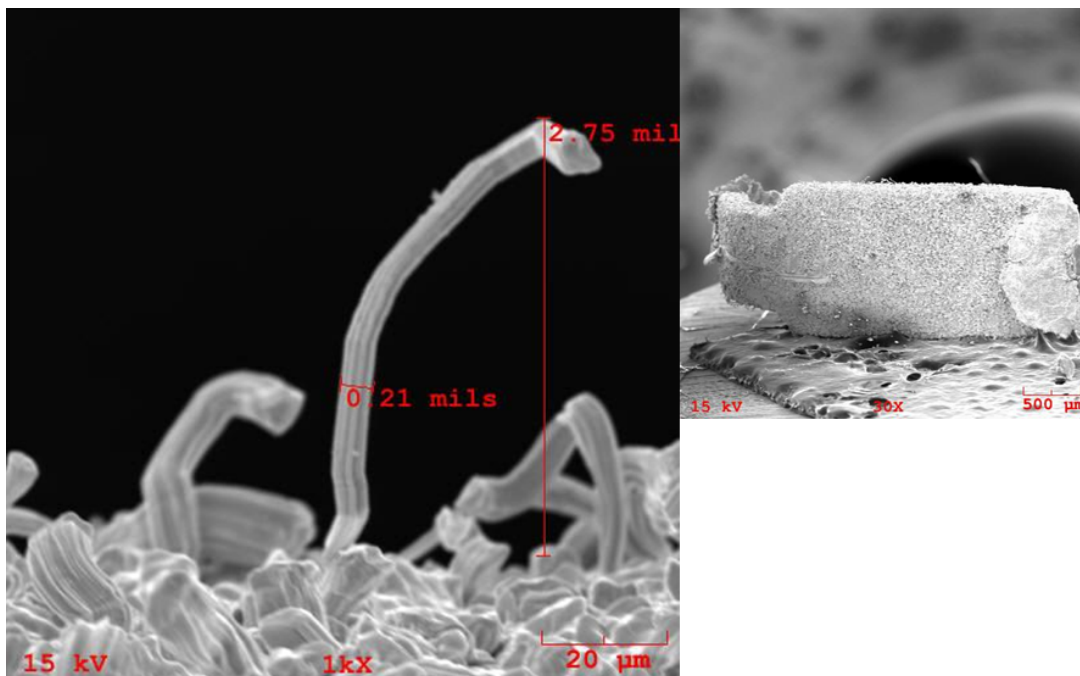
Sample 2
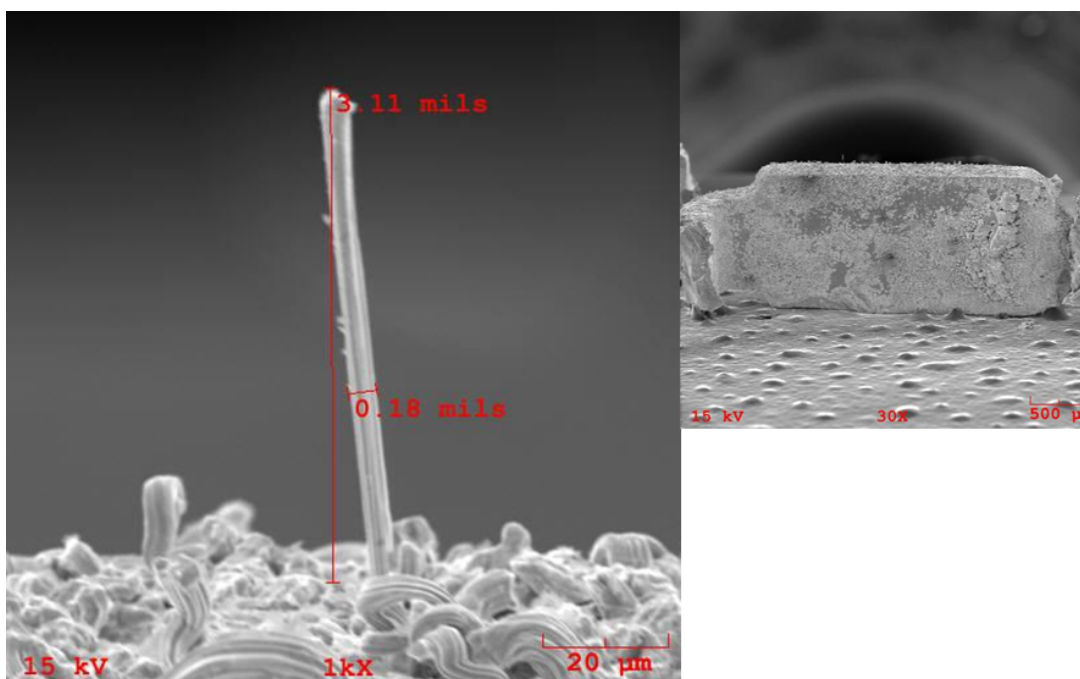
Sample 3
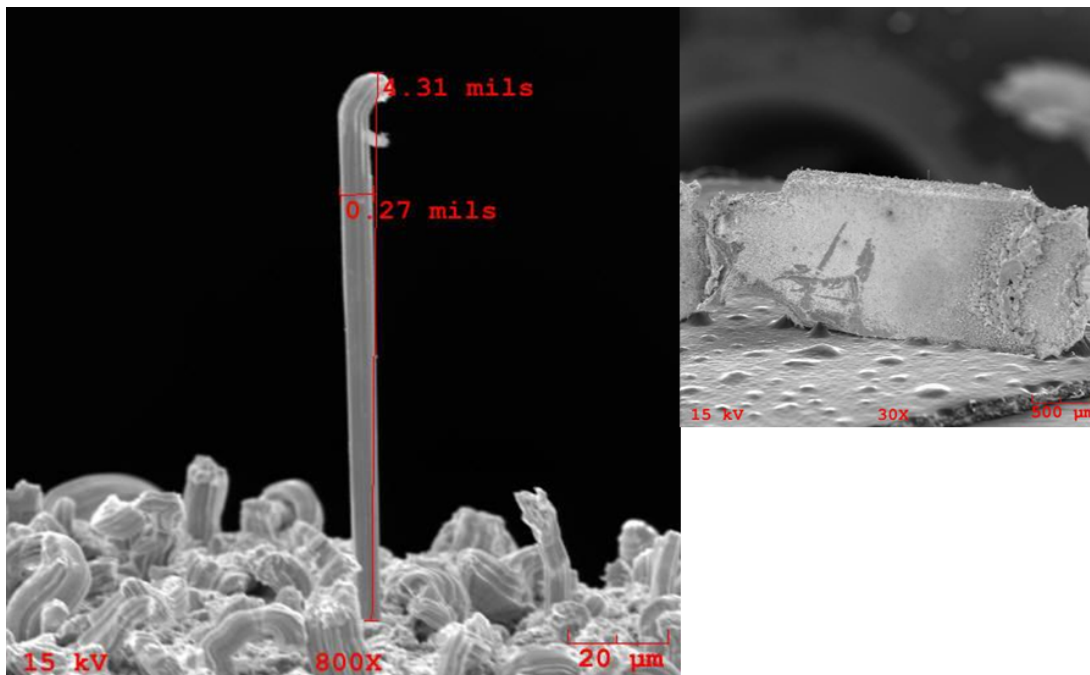
Sample 4
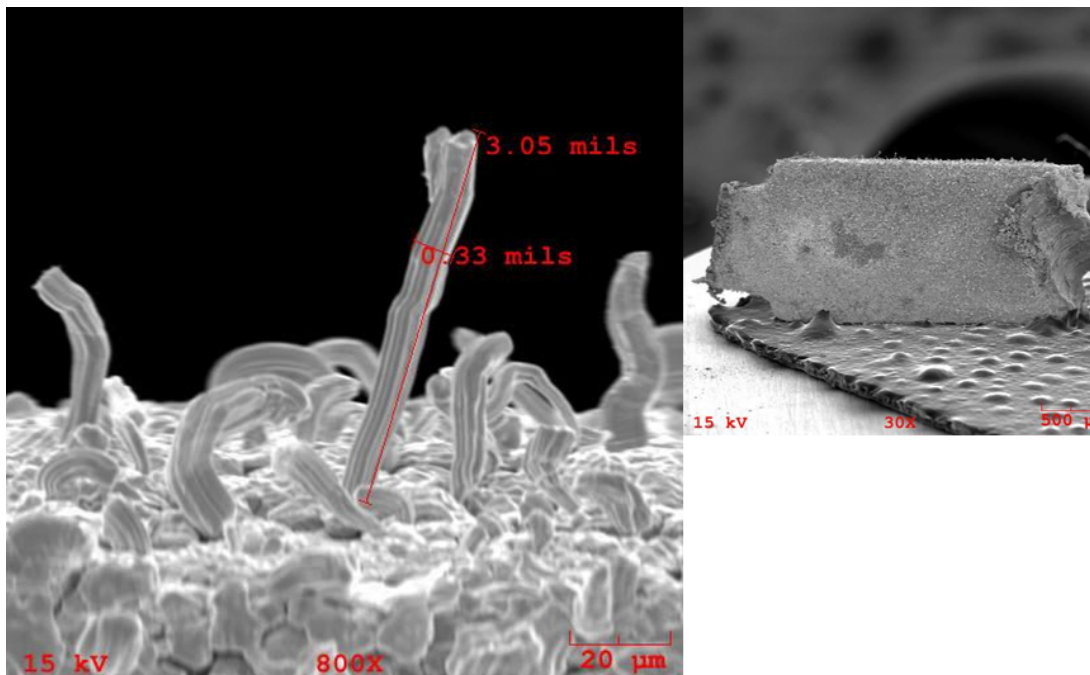
Sample 5
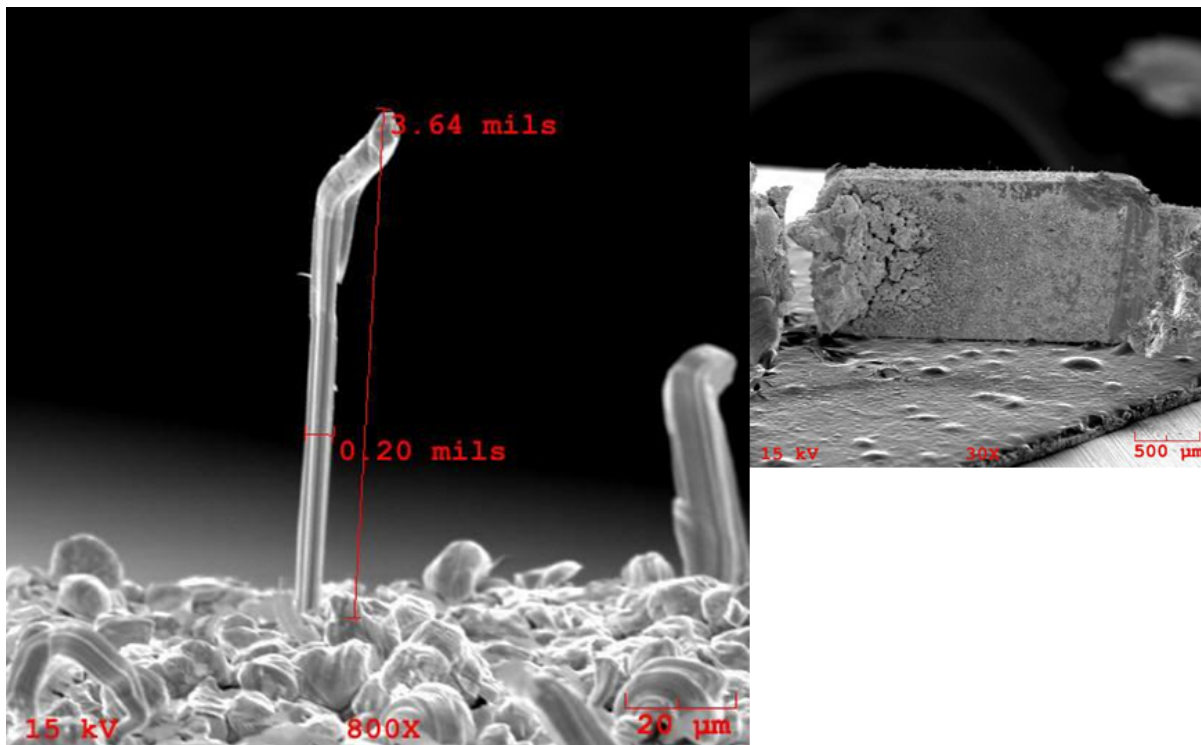
Sample 6
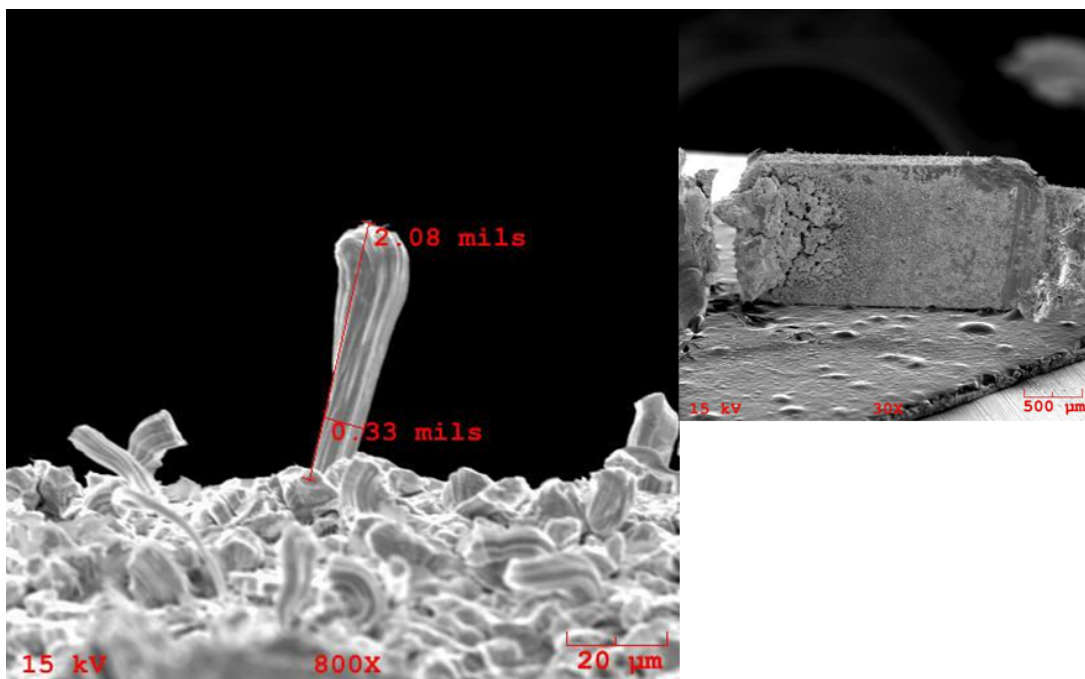
Sample 7

Scale measured from images
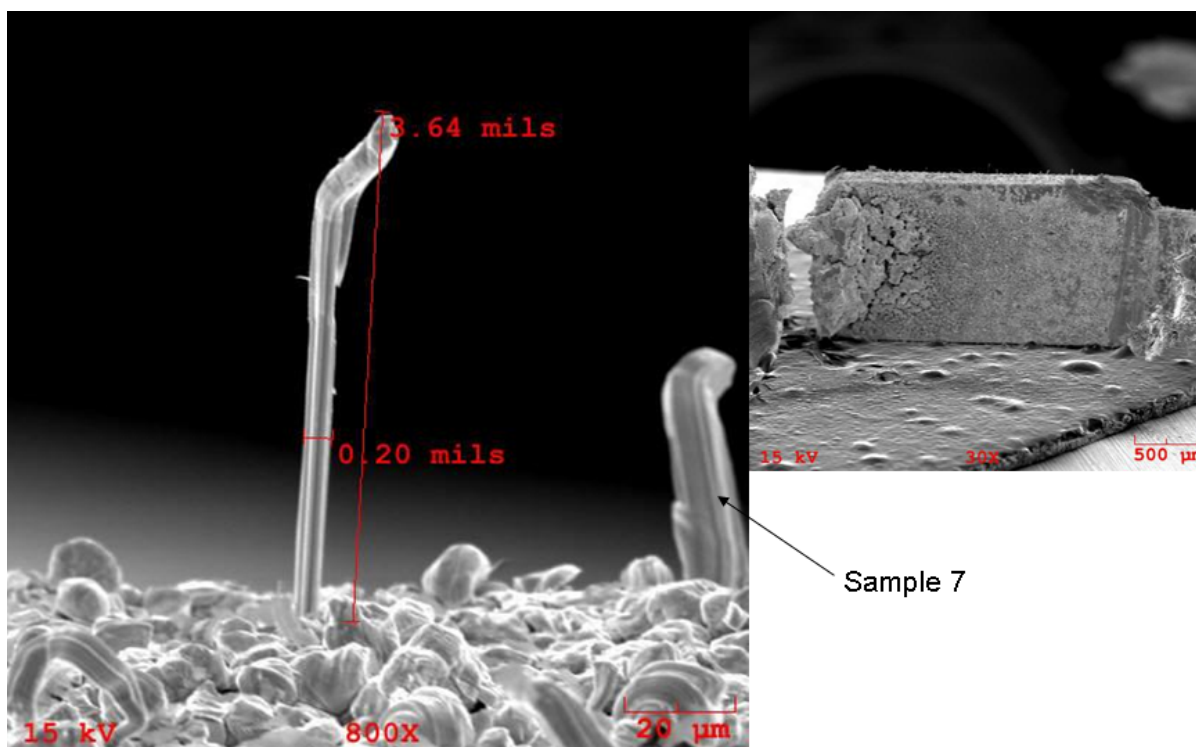
Sample 7

Appendix C   Microtribometer Sample Images and Force

Sample 1

Initial Contact   Mid Contact
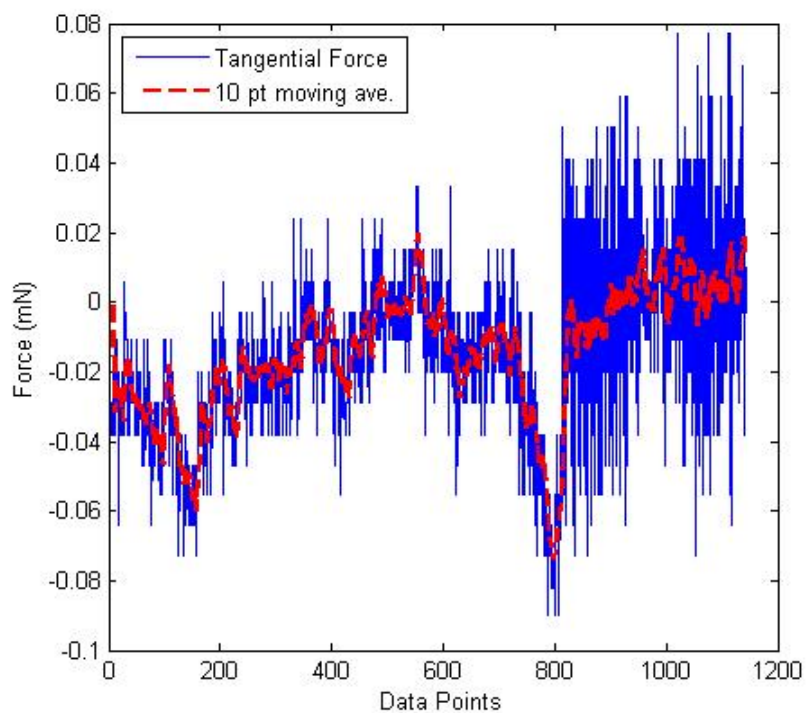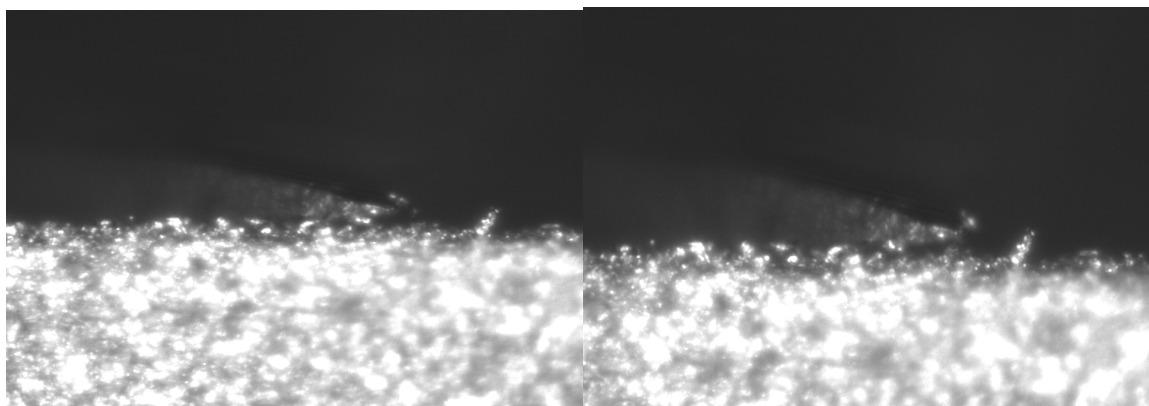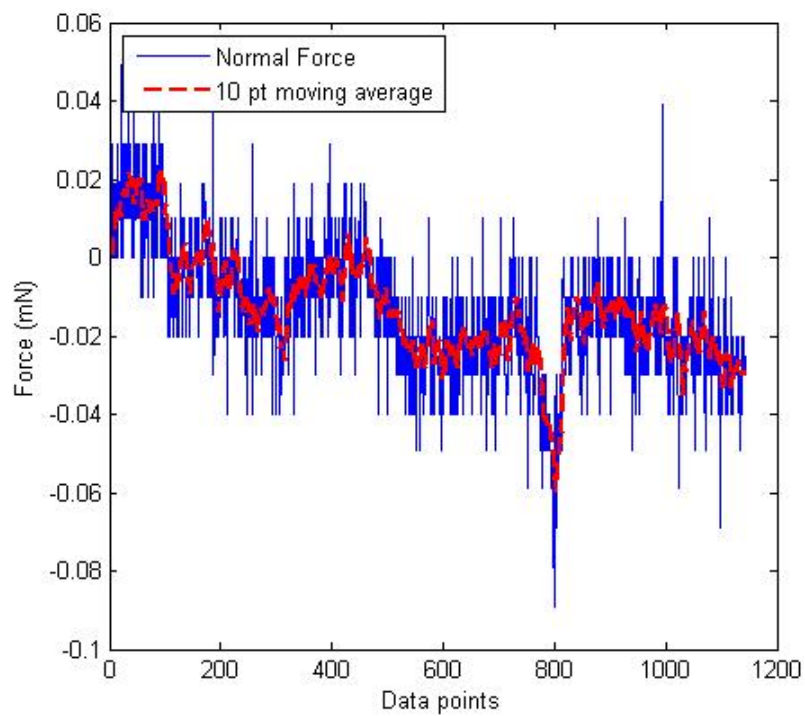
Sample 2

Initial Contact   Mid Contact
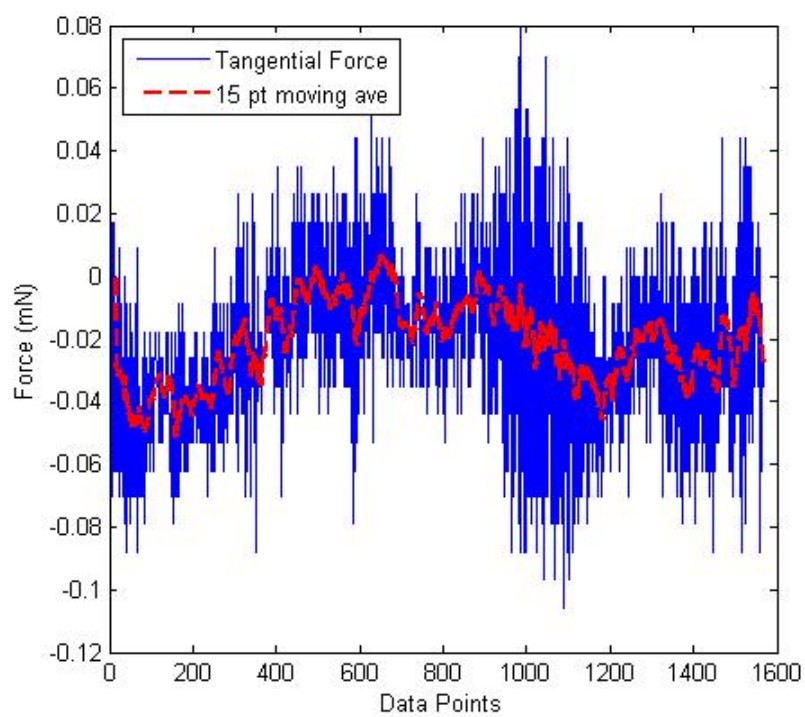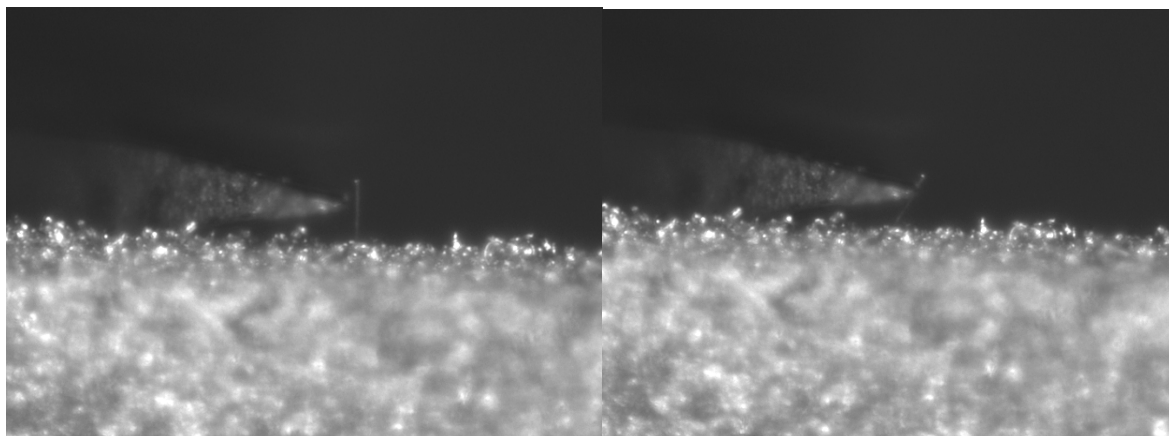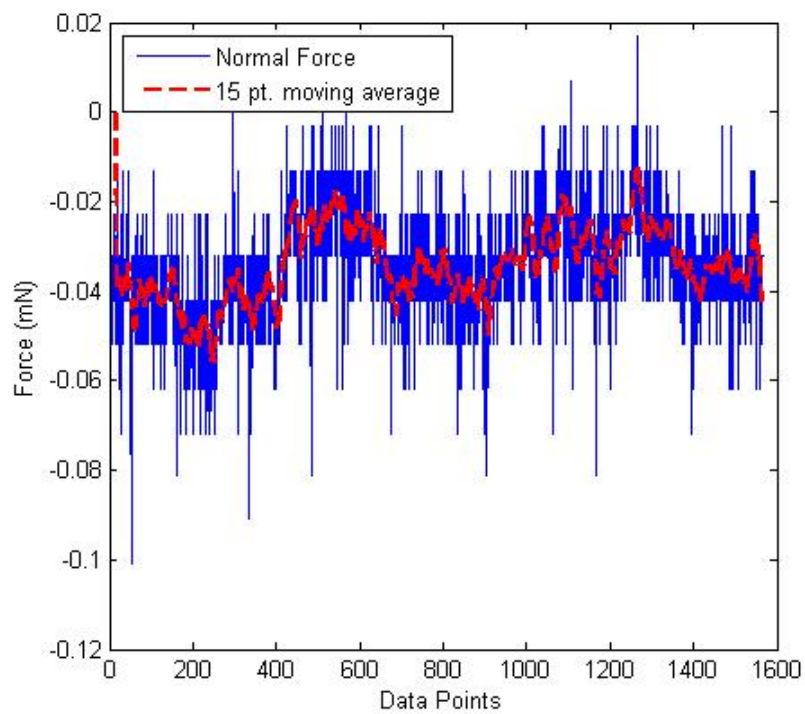
Sample 3

Non Contact Method
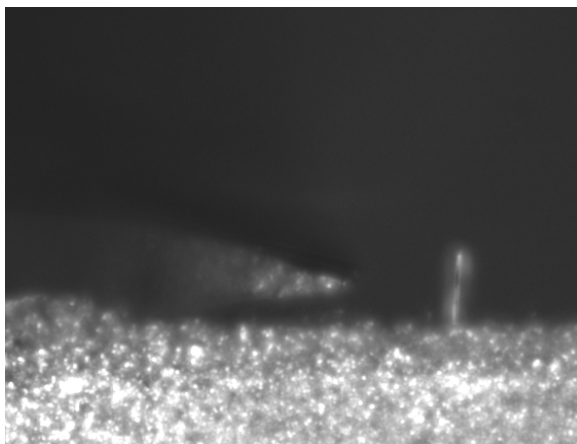
<div style="text-align:center">Alignment   Initial Contact</div>
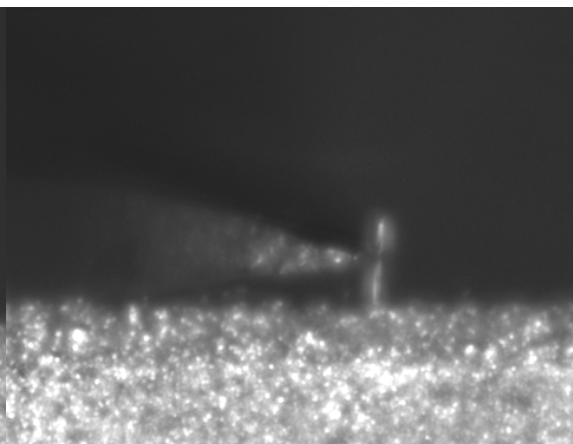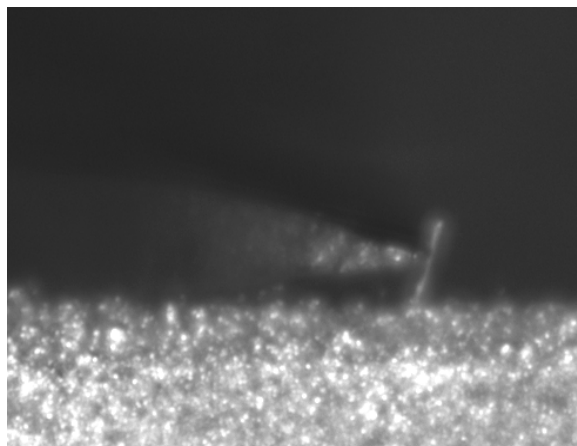
<div style="text-align:center">Mid Contact   End Contact</div>
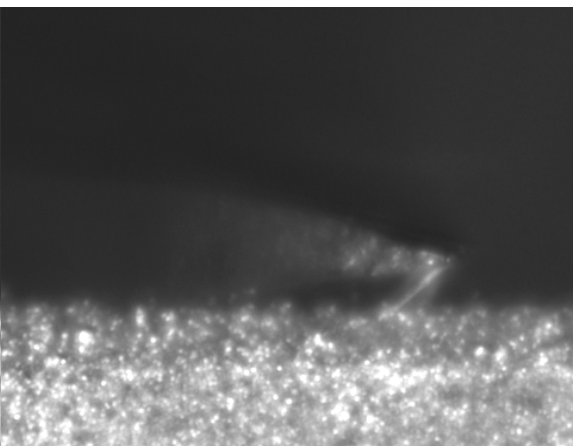
Contact (sliding) Method
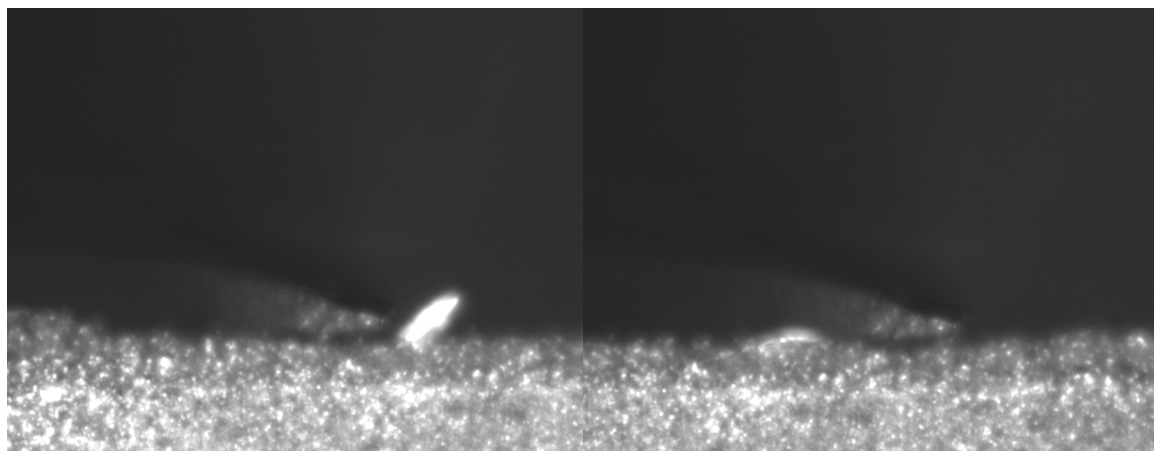
Non Contact Method
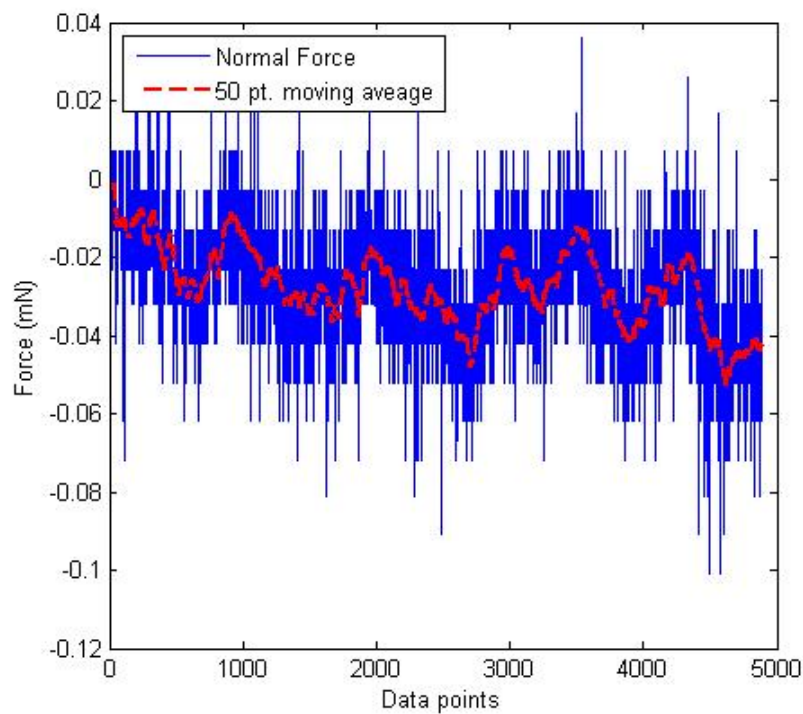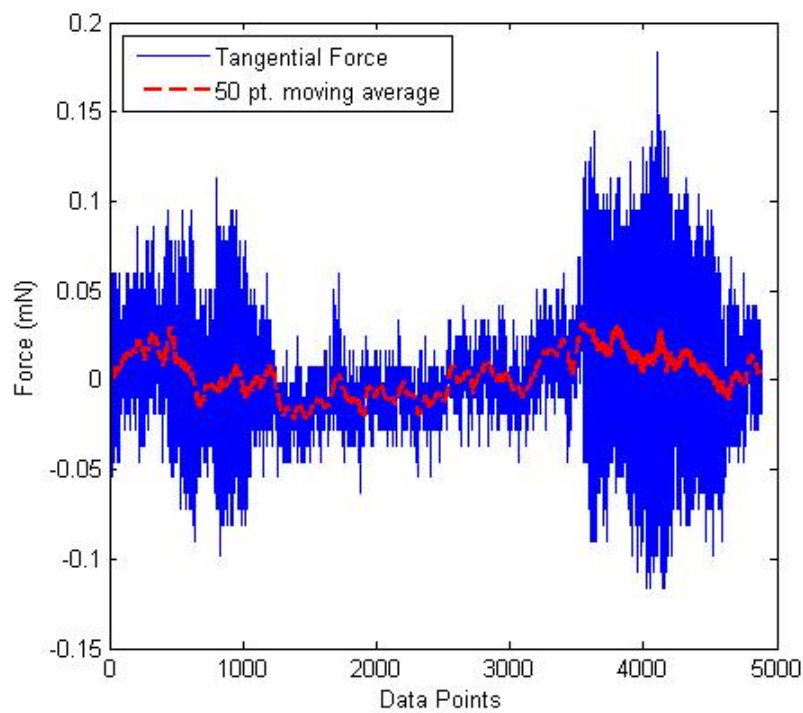
Contact (sliding) Method
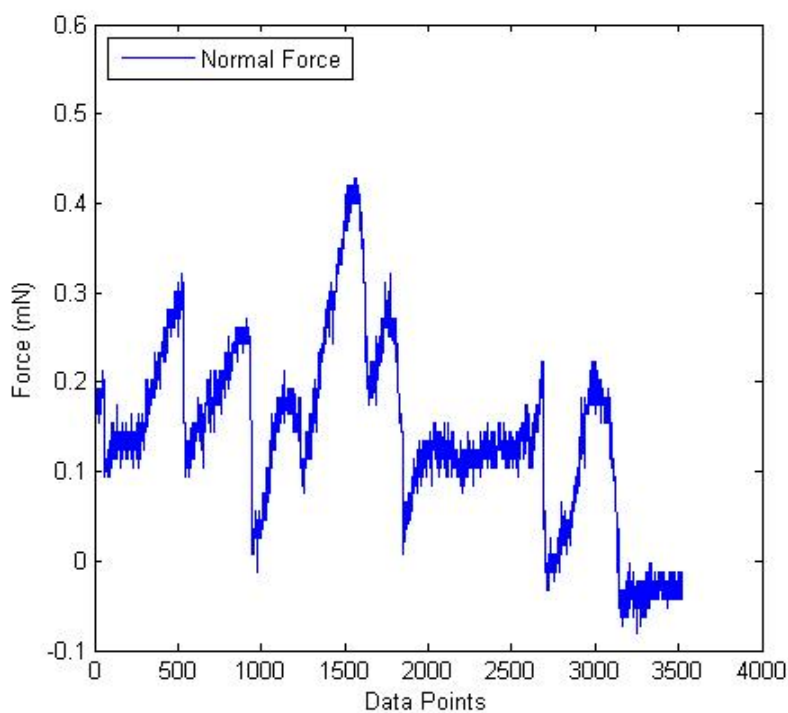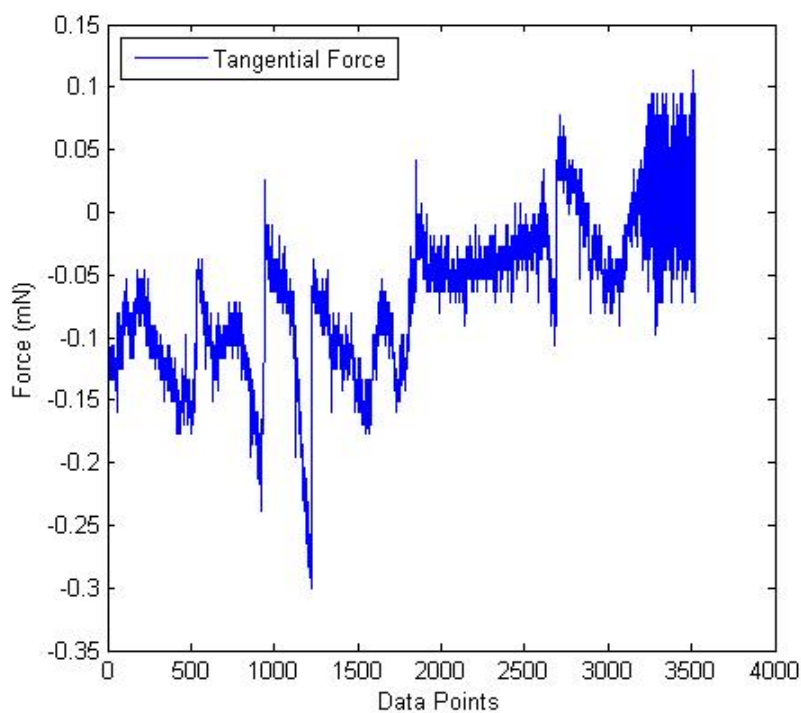
Sample 4

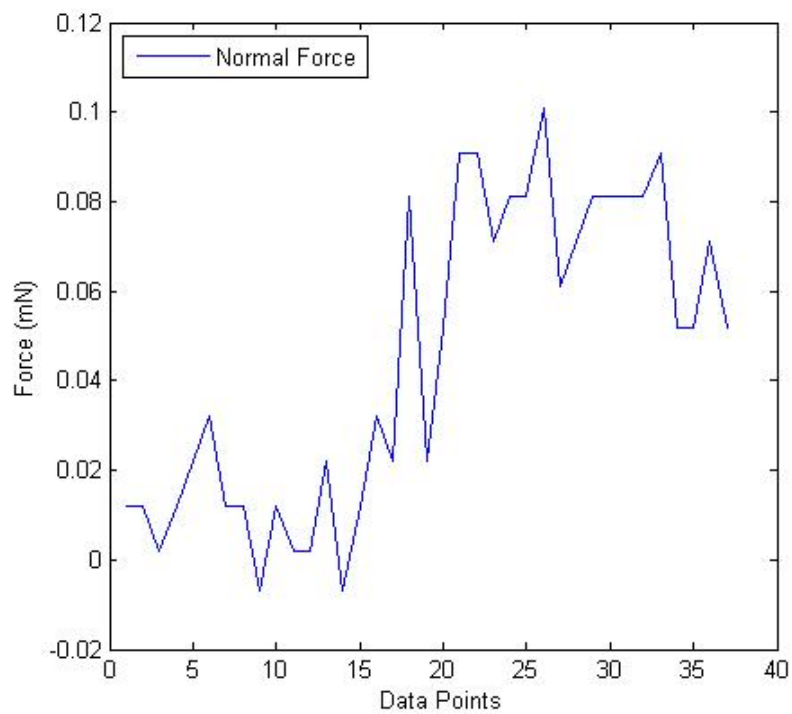Initial Contact   Post Contact
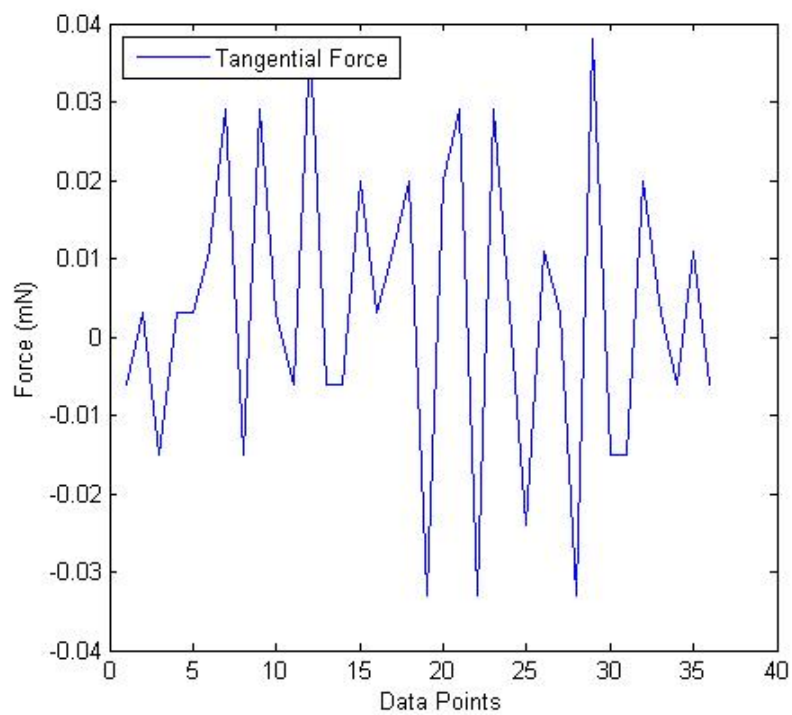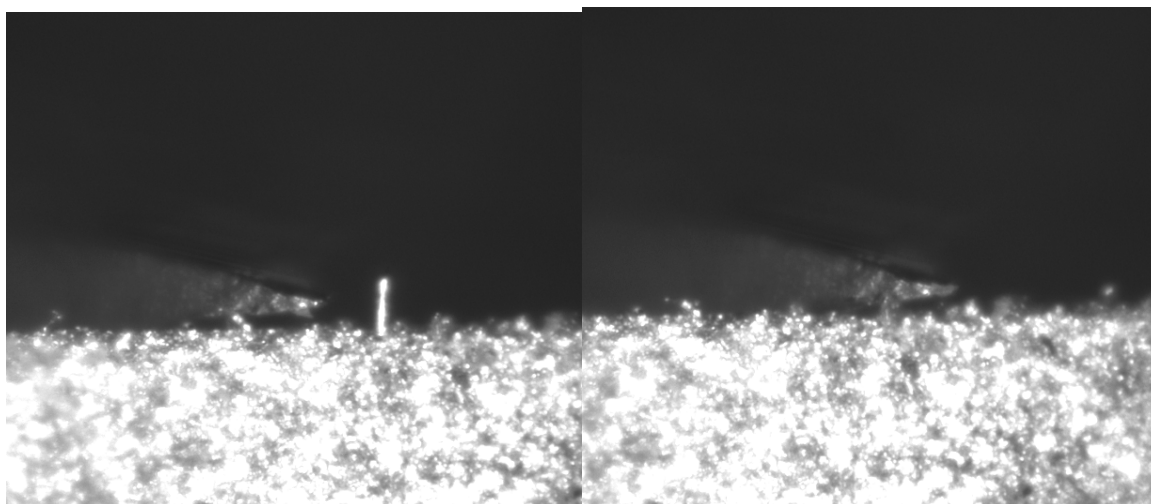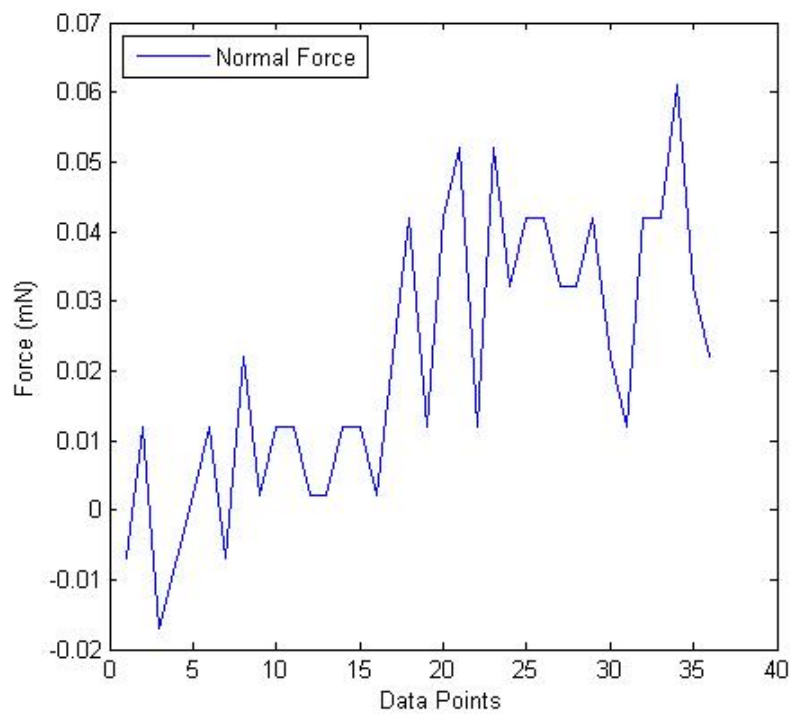
Sample 5

<div style="text-align: center;">

Initial Contact   Post Contact

</div>
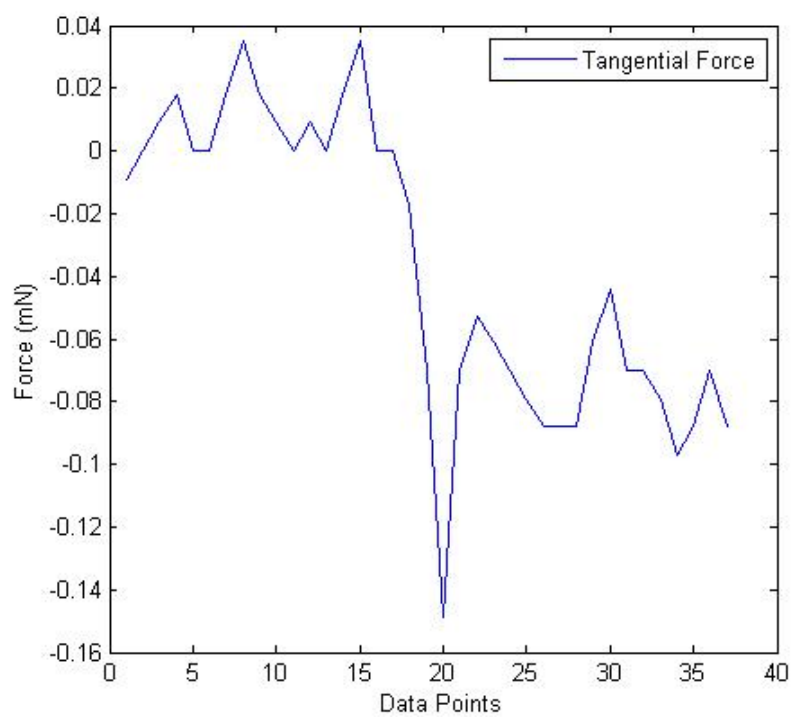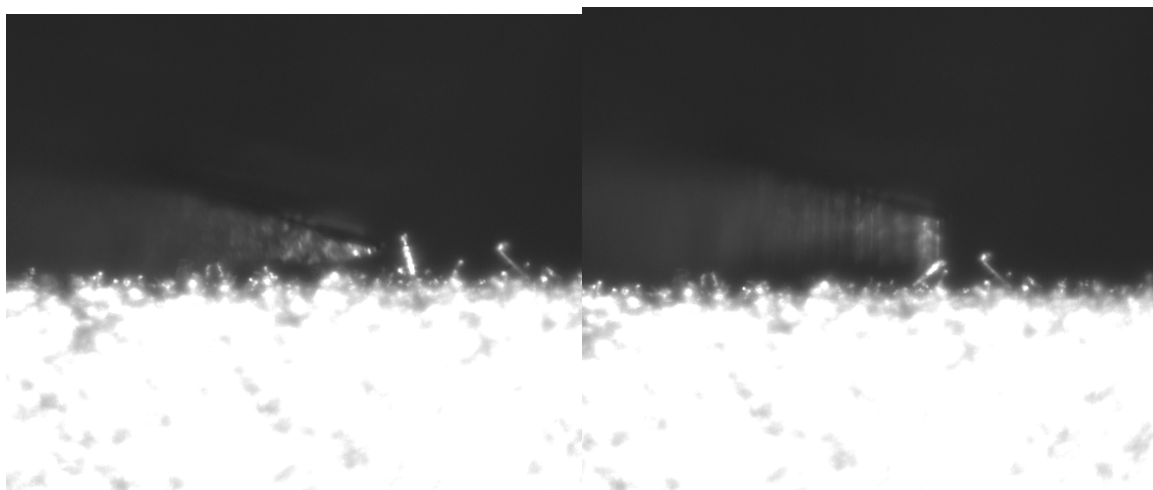
Sample 6

Initial Contact   Post Contact

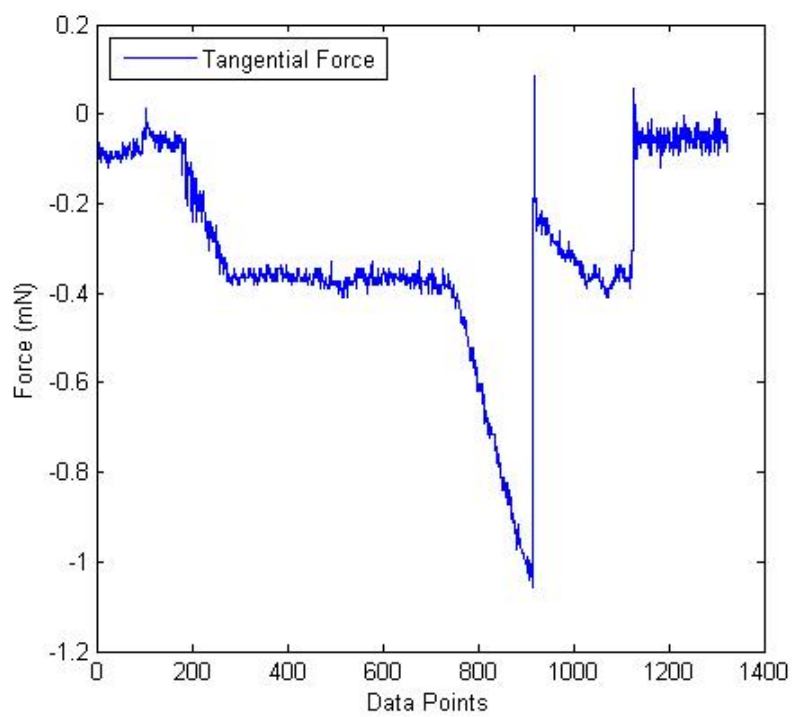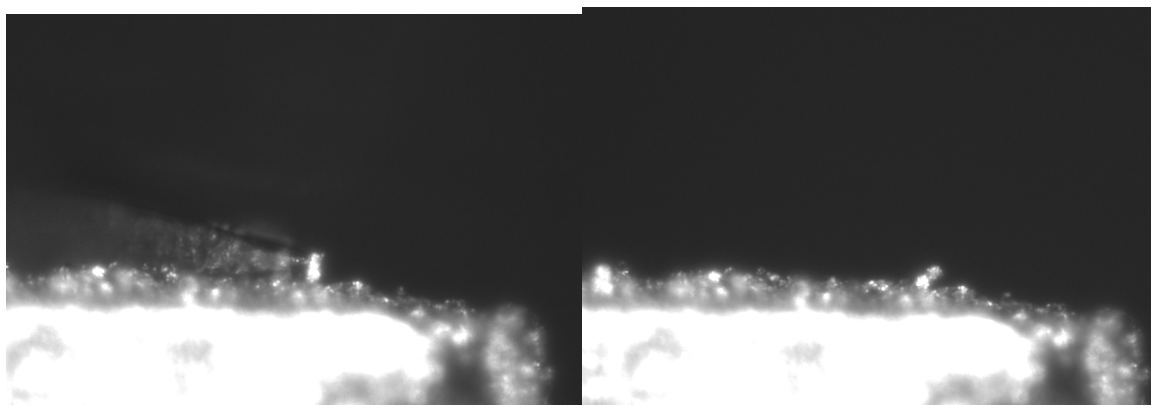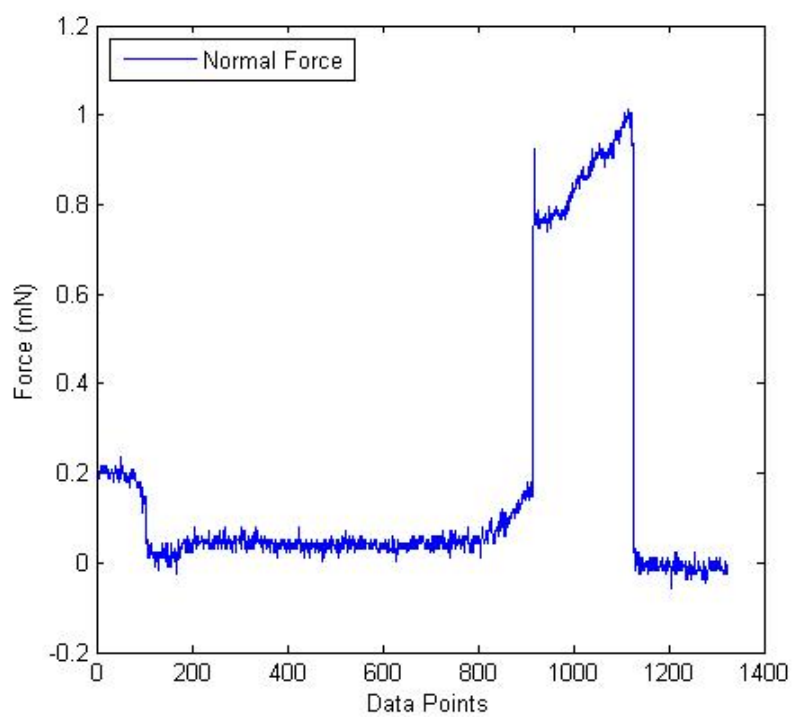**Sample 7**

Initial Contact   Post Contact